ISSN 0280-5316
ISRN LUTFD2/TFRT--5742--SE

Modeling and Control of a Large Deformable Mirror

Fredrik Bjöörn
Olof Garpinger

Department of Automatic Control
Lund Institute of Technology
April 2005

Department of Automatic Control
Lund Institute of Technology
Box 118
SE-221 00 Lund Sweden

Document name
MASTER THESIS

Date of issue
April 2005

Document Number
ISRN LUTFD2/TFRT--5742--SE

Author(s)
Fredrik Bjöörn and Olof Garpinger

Supervisor
Torben Andersen at Lund Observatory
Gustaf Olsson at IEA, Lund
Anders Robertsson at Automatic Control, Lund

Sponsoring organization

Title and subtitle
Modeling and Control of a Large Deformable Mirror. (Modellering och reglering av en stor deformerbar spegel)

Abstract
The current generation of earth-based telescopes has been of great use to astronomers for the past decades. New fields of astrophysics like the search for and analysis of earth-like planets would however need telescopes with even better resolution. These telescopes are called Extremely Large Telescopes and an ongoing project to develop such a telescope is the Euro50 project. For the Euro50 telescope to achieve enough resolution it will need an adaptive optics system with a large deformable secondary mirror to compensate for atmospheric disturbances. This will make the telescope images sharper. The shape control for such a large mirror requires a dynamic control approach. Since no real mirror was at hand, a modal state space model of the mirror was developed and controlled in the Matlab/Simulink environment. The final MIMO controller uses a combination of state feedback control and compensation filters.
This thesis was made in cooperation with Lund Observatory (Lund University), the Department of Automatic Control and the Department of Industrial Electrical Engineering and Automation (Lund Institute of Technology).

Keywords

Classification system and/or index terms (if any)

Supplementary bibliographical information

ISSN and key title
0280-5316

ISBN

Language
English

Number of pages
100

Recipient's notes

Security classification

Acknowledgments

The authors would like to thank their supervisor Torben Andersen at Lund Observatory for his help and invaluable knowledge of telescope control. Further a special thanks to our supervisors Gustaf Olsson and Anders Robertsson at Lund University for their expertise within the field of Automatic Control. Without the assistance from Holger Riewaldt a model of the deformable mirror would have been complicated to retrieve. Also lots of thanks to our co-workers Olof Sandberg and Roger Svahn for their good spirit and support during the late nights finishing our theses.

Contents

1 Background **7**
1.1 Extremely Large Telescopes 7
1.2 The Euro50 project 8
1.3 Adaptive Optics 9
1.4 The Euro50 deformable mirror 12
1.5 Different deformable mirror control approaches 15
1.5.1 Classic control of deformable mirrors 15
1.5.2 SISO control of a secondary mirror 15
1.5.3 Global MIMO control of a deformable mirror 17
1.5.4 Conclusions for the Euro50 mirror control 18

2 Introduction to the Euro50 Control **19**
2.1 The control in general 19
2.2 The control of the deformable mirror 20
2.3 Thesis goals and control specifications 22

3 Modeling a Deformable Mirror **25**
3.1 Theory on modal modeling 25
3.1.1 The 2002 modal model 27
3.2 Verification of the mirror model 29
3.3 Other mirror models 35
3.3.1 A Guyan reduced mirror model 35
3.3.2 A local mirror model 35

4 The Control of a Large Deformable Mirror **37**
4.1 Stability and robustness 37
4.1.1 Phase margin 37
4.2 System compensations 38
4.2.1 Lag filters 38
4.2.2 Lead filters 39
4.2.3 Band pass filters 40
4.3 SISO control of the deformable mirror 41
4.3.1 Transfer functions for the individual actuators 41
4.3.2 SISO control using compensation filters 42
4.3.3 Results of the individual control 44
4.3.4 SISO control of the full mirror 46
4.4 Local control using a static force distribution 47
4.4.1 Strategy of local control 47
4.4.2 Results of the local control 50

4.5 Local control of the full mirror model 50
4.5.1 Control development 51
4.5.2 Implementation of the full mirror control 52
4.5.3 Results of the full mirror control 54
4.6 Control using state feedback 57
4.7 Control using modal damping 59
4.8 Control evolution results 61
4.9 State feedback control with higher bandwidth 64
4.10 Control difficulties 66
4.10.1 Fast control and model reliability 66
4.10.2 Cumbersome simulations 68

5 Recommendations on future research 69

6 Main results and conclusions 71

References 73

A Matlab programming files 75
A.1 State space modal model derivation 75
A.2 Verification of the mirror model 77
A.3 Transfer functions for the actuators 81
A.4 SISO compensation filters for the actuators 83
A.5 Create a movie of the mirror 87
A.6 Initial file to test full mirror step responses 88
A.7 Place forces on the deformable mirror 95

1 Background

The main purpose of this chapter is to give a short introduction to the next generation of telescopes and their need for an adaptive optics system. Furthermore, tools and control systems needed for the adaptive optics to operate will be discussed. All will be viewed in background to the Euro50 project.

1.1 Extremely Large Telescopes

The largest earth-based mirror telescopes of today are the so-called Very Large Telescopes (VLTs) with primary mirror[1] diameters of about 10 meters. Although their usefulness have been immense to astronomers during the past decade, there is today a need for even larger telescopes. Science fields of interest like the early universe, the expansion of the universe and the evolution of galaxies are all requiring new telescope knowledge to become available. Another exciting new field of science is the search for earth-like planets. The number of external planets that are known to us are growing rapidly, but these planets are all very big, like the gas giants in our own solar system (e.g. Jupiter and Saturn). Although one may also soon be able to locate earth-like planets it does not necessarily mean that one will be able to study them in much detail[2].

For studies like those mentioned above to become available, a new generation of telescopes needs to be developed. This new generation of telescopes will have primary mirror dimensions of 30 to 100 meters in diameter. These are the so-called Extremely Large Telescopes (ELTs). For an earth-based telescope of this size to be efficient it should have an optical system that includes a fast, adjustable, primary mirror and an adaptive optics system. The flexible primary mirror enables the telescope to keep an optimal focus and a steady aim at the target of observation. The reason to have an adaptive optics system is to compensate for disturbances that the atmosphere is adding to incoming radiation from the universe. Since adaptive optics is a major part of this thesis it will be dealt with in more detail later.

[1] Most optical telescopes use a primary mirror to gather light and reflect it to a secondary mirror which focuses it. See the primary mirror in Figure 1 and the beam path in Figure 2.

[2] Those interested in Astronomy can for instance see [4], [9]

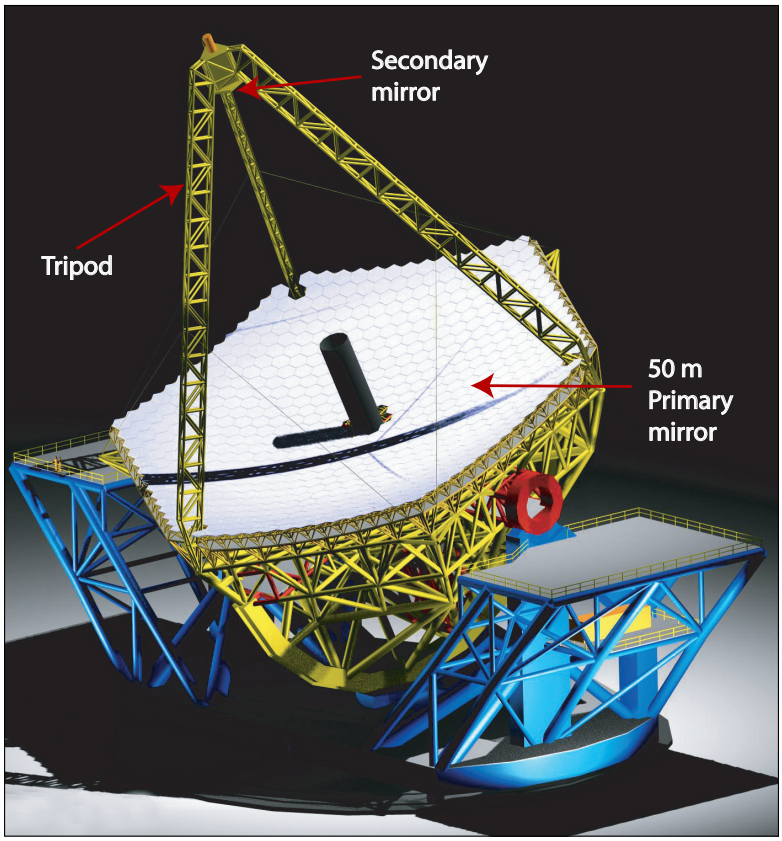

Figure 1: The Euro50 Telescope [3]

1.2 The Euro50 project

As there is an obvious interest in developing Extremely Large Telescopes, several groups are involved in such projects today. One of these project groups is the Euro50 group which consists of scientists from Finland, Ireland, Spain, United Kingdom and Sweden. The Euro50 telescope[3] (see Figure 1) will weigh approximately 3500 tons and measure about 90 meters from top to bottom. The name of the telescope emanates from the dimension of the hexagonal primary mirror, which will have an equivalent diameter of 50 meters. The Euro50 primary mirror will consist of 618, 2 meter edge-to-edge, hexagonal mirror segments. The optical arrangement for the telescope is of so-called aplanatic Gregorian type with a 4 m edge-to-edge secondary mirror. This secondary mirror is placed on the top of a tripod structure (see Figure 1) and is used to focus the light reflected by the primary mirror.

[3]For more information on the Euro50 telescope, see [3], [6]

The use of an adaptive optics system will increase the angular resolution[4] of the telescope to about 2-3 milliarcseconds in visible light and to 10 milliarcseconds in Infrared (IR) light. This is about 200 times better than any of today's telescopes, without adaptive optics technology, are capable of. The adaptive optics system is obviously of great importance, but how does it work?

1.3 Adaptive Optics

Light waves[5], for example from a distant star, traveling through space are parallel when they reach the atmosphere of the earth. Turbulence in the atmospheric layers leads to different refractive indices over the wavefront (see Figure 2). The effect that this has on the wavefront is called distortion and it blurs images created by telescopes on Earth. If the distortion could be compensated for, the only limit in the angular resolution of astronomic images would be that of diffraction which is always present. One way to solve this problem is to place a telescope above the atmosphere like the Hubble Space Telescope (HST). However, building and maintaining a telescope like the HST is far more expensive than the costs of an Earth-based telescope like the Euro50. An alternative to a space telescope is a telescope which uses so-called adaptive optics to compensate for atmospheric distortion.

Adaptive optics is the adaptation of the telescope optical system and works as follows. Measurements of incoming light from natural and artificial stars[6] give information on the nature of the atmosphere at a certain point in time. The information most often used is the phase of the incoming light over a certain area, which gives a measure of the distortion. The instruments used for this purpose are called wavefront sensors. The Shack-Hartmann wavefront sensor, for instance, uses so-called lenselet arrays to focus different parts of the wavefront onto several CCD-cameras whose intensity pattern gives a measure of the phase. A map of the wavefront phase pattern, at a certain point in time, can then be created. This is called reconstruction.

[4]The angular resolution of a telescope is a measure of the sharpness of the telescope images. Low resolution gives blurry pictures. The resolution depends mainly on the primary mirror diameter which determines the light collecting area.

[5]It is common to view light as an electromagnetic wave, almost like the waves on the ocean. The peaks of the incoming light waves are called wavefronts.

[6]One can create an artificial star by exciting certain atoms in the atmosphere. These start to glow when lasers are aimed at them.

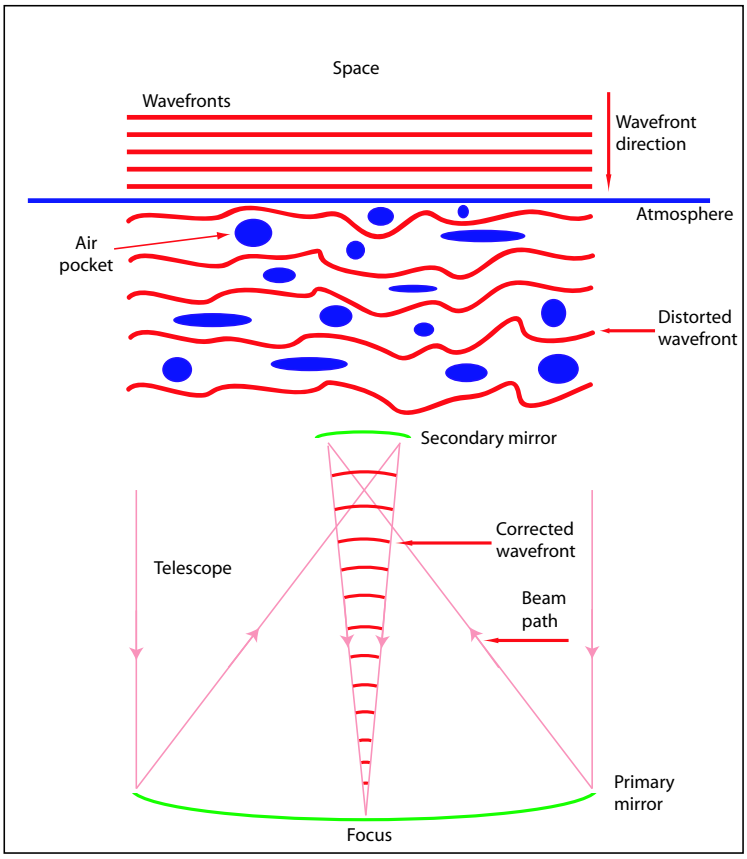

Figure 2: The incoming light wavefronts from e.g. a star are parallel when entering the atmosphere of the earth. Turbulence in the atmospheric layers creates pockets of air, with different refractive indexes, distorting the light. The distorted light is compensated for by a deformable mirror and the light focused is parallel (or spherical) resulting in a sharper image.

According to Figure 2, atmospheric disturbances can also be viewed as differences in the optical path length for the wavefront. The most common way to compensate for these path differences is to use a deformable secondary mirror in the telescope. A deformable mirror is a flexible structure whose surface can be shaped dynamically into a custom form. This has the advantage that one can minimize the path length differences in the incoming light, as in Figure 3. The incoming light falls onto the mirror which in turn is deformed into the shape producing a straight wavefront leaving the mirror. Finally, parallel (or spherical) wavefronts, coming from the secondary mirror, will be focused to create an image of the astronomic object, see Figure 2. This is how adaptive optics work and the difference in resolution between a telescope

using an adaptive optics system and one that is not, can be seen in Figure 4.

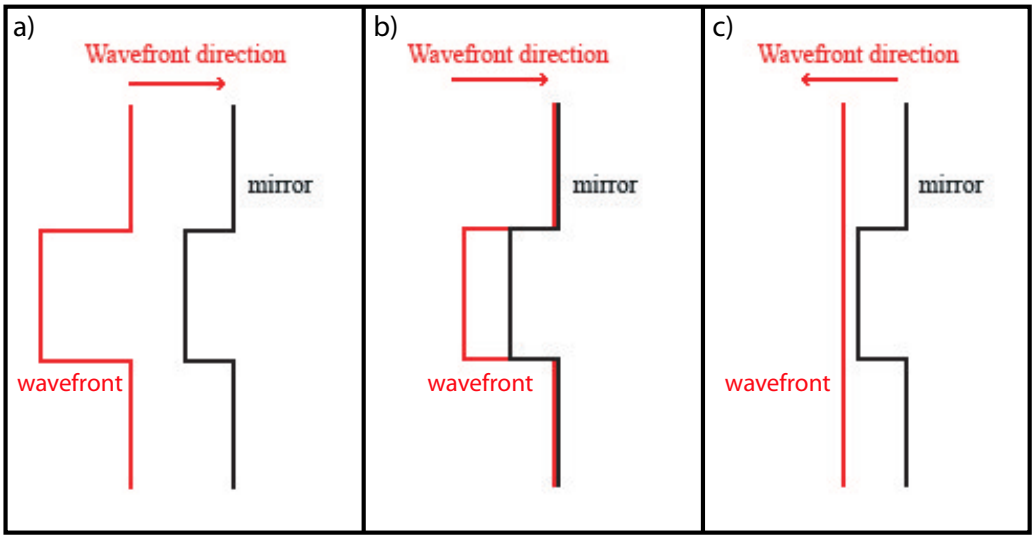

Figure 3: a) A distorted wavefront is approaching the deformable mirror which has changed its shape accordingly. b) The front part of the wavefront is forced to take a longer path than the rest, before it reflects off the mirror. c) The mirror has corrected for the differences in optical path length of the wavefront and a straight wavefront leaves the deformable mirror, [11]. Note that a wavefront is normally continous. The shape of the wavefront was used only clarify the purpose of the deformable mirror.

For a deformable mirror to be able to change its shape it has to be influenced by forces. These forces are created by actuators placed on the back of the mirror. To achieve a mirror shape with enough resolution a large number of actuators will have to be used. The resolution that has to be reached is higher for shorter wavelengths. The Euro50 is planned to use 3168 actuators for IR-light but will need many more when dealing with visible light. The studies of this thesis however, are only concerned with the 3168 actuator problem.

The Euro50 telescope will also need a very large deformable mirror. Large deformable mirrors have more eigenfrequencies within the band of control than small ones. Therefore, small mirrors can be approximated as only statically influenced by the actuators. This, on the other hand, is impossible for the Euro50 approach and the actuators will therefore need to control the mirror shape dynamically to compensate for mirror mode vibrations.

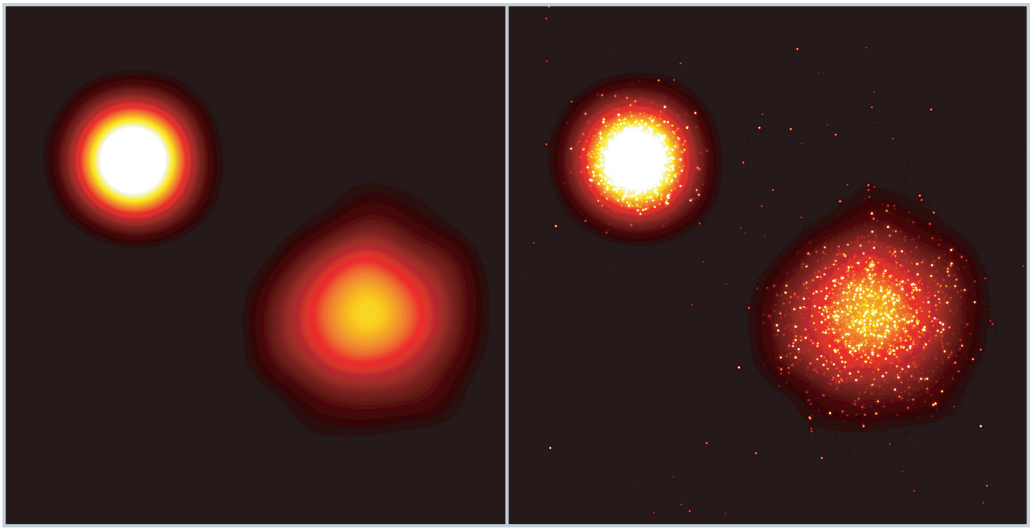

Figure 4: The picture to the left shows two star clusters and is taken by a telescope without an adaptive optics system. The picture to the right is showing the exact same clusters, but is taken by a telescope with an active adaptive optics system. It should be mentioned that the pictures are the result of a simulation [6].

For more information on adaptive optics see [2], [11].

1.4 The Euro50 deformable mirror

The Euro50 secondary mirror is a 2 mm thick mirror with a concave hexagonal shape, see Figure 5. The mirror should be as thin as possible to decrease the total weight and make the actuation more efficient. It will be made of Carbon Fiber Reinforced Polymer (CFRP) which is a lightweight material made of a sequence of different fiber layers. The hexagonal mirror shape is merely a result of the primary mirror form. The deformable secondary has an equivalent diameter of 4 m making it much larger than any deformable mirror used in telescopes today.

A finite element model of the secondary mirror, derived at Lund observatory, determined most of its dynamic properties. An important part of this model was the eigenmodes[7] of the mirror which will have to be handled by the dynamic control. The CFRP material gives a poor modal damping ratio of

[7]The eigenmodes are natural mirror shapes formed when triggered by the mirror eigenfrequencies. The eigenfrequencies are resonance frequencies, i.e. frequencies the system tend to oscillate with.

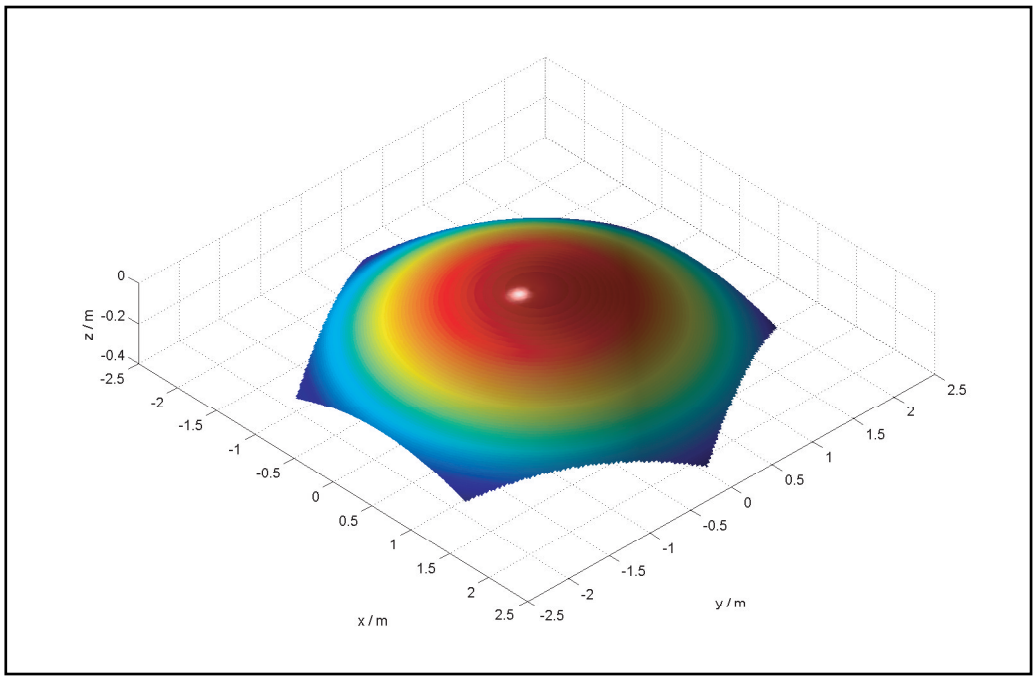

Figure 5: The Euro50 deformable mirror shape.

about 0.02 which makes it difficult to control. The fast atmospheric changes place further demands on the mirror control to work with a frequency of about 500 Hz. Since the highest mode frequencies are much higher than this, some of the modes can be disregarded. The diagram in Figure 6 shows the eigenfrequencies of the modes used in a 2002 mode model that will be described later. Only the first 2002 modes were used to make this model. Those modes with even higher frequencies were simply truncated. Another thing to notice is that there are many more eigenfrequencies above 200 Hz than below. There are two different types of eigenmodes present below 200 Hz, i.e. circumferential and radial modes. The eigenmodes above this frequency are both circumferential and radial. Some of the 2002 eigenmodes can be viewed in Figure 7. Note that it is the actual shape of the mirror that is plotted. The dimensions are the same as in Figure 5.

The full mirror model includes many more than 2002 modes, some of which are more significant than others. This fact will be used in another model that will focus on the important modes or degrees of freedom. This enables us to use the model at higher frequencies still having almost the same model size. The significance of modes will also be considered in the mirror control.

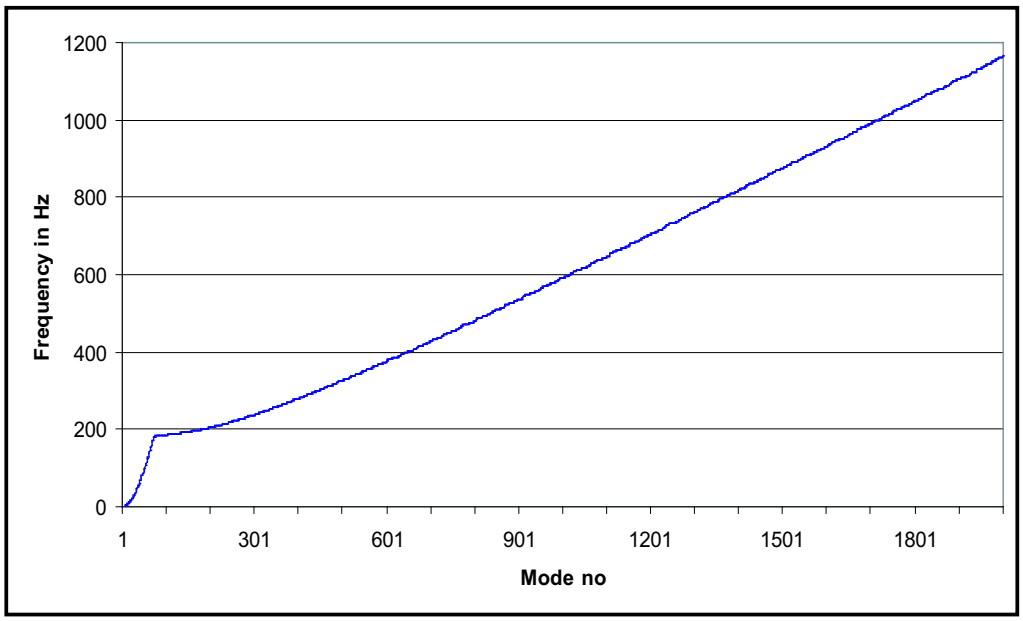

Figure 6: The eigenfrequencies of the first 2002 modes in the finite element model.

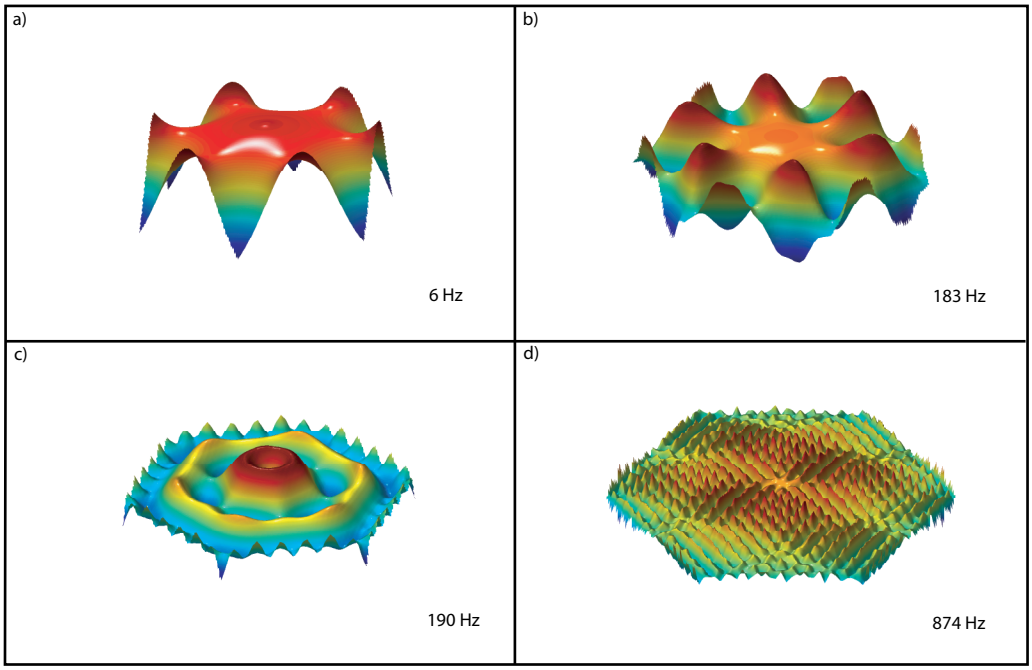

Figure 7: Four deformable mirror eigenmodes. a) Mode number 11 b) Mode number 81 c) Mode number 131 d) Mode number 1501.

1.5 Different deformable mirror control approaches

The control of deformable mirrors is a young branch of technology. This means that it is quite hard to find good sources with hints as to how the Euro50 mirror can be controlled properly. There are however a few examples worth mentioning.

1.5.1 Classic control of deformable mirrors

The oldest way to maneuver a deformable mirror is to assume that the deformations of the mirror are almost static in the region of control, so-called quasi-static. The signals from the wavefront sensors are reconstructed into deformation command signals to the mirror control. Depending on whether the actuators are stiff or not, the mirror shape will vary when influenced by forces. The influence function of an actuator is a shape function that the mirror surface around the actuator will take when subjected to the actuator force. If the neighbour actuators are stiff the influence function will be narrow, which is due to the actuators' unwillingness to change shape. For actuators with low stiffness the opposite holds. They are willing to stretch and thereby allow the mirror to deform freely.

If the influence functions for all mirror actuators are added, then one will know exactly what forces are needed to shape the mirror properly. Simple proportional controllers for each actuator should then be sufficient to control the entire mirror surface. This control approach, however, is not applicable for the Euro50 secondary mirror control. As mentioned before, only a mirror of small enough size can be approximated as quasi-static. These mirrors have few or no eigenmodes within the range of control. The Euro50 mirror on the other hand, has many and can not be viewed as quasi-static.

1.5.2 SISO control of a secondary mirror

The Multiple Mirror Telescope (MMT, see Figure 8) is situated on Mount Hopkins in Arizona, USA ([1]). It has a primary mirror with a diameter of 6.5 m and a deformable secondary mirror with a diameter of 64.2 cm. The adaptive optics system has been developed by a group of Italian scientists ([7], [8]). Their secondary mirror is controlled by 336 actuators, all fed back by as many capacitive gap sensors measuring the deformations of the mirror. The sensors are collocated with the actuators on a reference plate just above the mirror. The reference plate produces an air gap, damping the mirror modes. This modal damping simplifies the control of the secondary mirror. Note the difference between a mirror with damping ratio $\zeta = 0.02$, which

Figure 8: The Multiple Mirror Telescope (`http://www.sao.ru/hq/komarov/tel/06/big.htm`)

is the case for the Euro50, and a well damped system with $\zeta = 0.7$. The resonance frequencies of the last system are much easier to control, since the transfer functions are then approximately second order low pass filters. The high benefit is that Single Input Single Output (SISO) PD controllers can be designed for each actuator using only the deformation at the same position as the feedback signal. The exact same controller is then implemented on each and every actuator in locally closed loops. The first system (with $\zeta = 0.02$) has transfer functions with high resonance peaks and a fast-changing phase around the eigenfrequencies. In order to keep a mechanical simplicity, the Euro50 construction will not use an air gap for damping purposes. Electronic damping will be employed instead.

Since the number of actuators is very large for the MMT secondary, it is also important to keep the computer computations to as few as possible without adding any unnecessary time delays to the system. A Multiple Input

Multiple Output (MIMO) system is much more demanding than the SISO alternative concerning design and computations.

It should also be mentioned that this SISO approach is currently used in the operating system in Arizona.

1.5.3 Global MIMO control of a deformable mirror

Another approach to the same control issue of the MMT secondary has been developed by Simon C.O. Grocott, PhD student at MIT [11]. Grocott uses the more time consuming MIMO control method in which he controls a model including both the deformable mirror dynamics and the dynamics of the atmosphere. He calls the control "global" because of the extended system model. This model has two noise inputs which originates from sensor noise and atmospheric disturbance. Grocott has used a MIMO version of the so-called Linear Quadratic Control to control this system. He has also made use of the fact that the MMT deformable, in contrary to the Euro50, is circular. This detail makes it possible to transform the model matrices into circulant matrices, thereby reducing both the order of the system and the number of computations necessary to perform the control. Throughout his work, Grocott has never presumed any modal damping, like the Italians have. As the Euro50 has no air gap to rely on either, Grocott's studies may be of great interest.

Simon Grocott has also made a thorough comparison between his Global LQG approach and the PD approach of the Italian group where he compares the benefits and drawbacks of the different designs. The main disadvantage of the global control approach is the cumbersome calculations involved in the determination of the MIMO system control law. The advantage, however, is that it evades some of the main problems when working with the SISO method. The problems that Grocott sheds light on are

- The SISO open loop system has no natural roll-off which leads to robustness problems for the closed loop. Time delays and model errors could be devastating. The D-part of the controller is also raising the high frequency gain.
- The same PD controller is used at every location on the mirror. The controller, on the other hand, is designed for one actuator alone. Another actuator location might have completely different dynamics leading to poor control.

- The deformable mirror system is highly coupled[8] which could lead to instability for the whole mirror although each SISO system may be stable individually.

1.5.4 Conclusions for the Euro50 mirror control

Since the Euro50 telescope has an even larger deformable mirror than the MMT, it seems important to consider Grocott's work. There is no modal damping and the larger dimensions of the Euro50 deformable mirror give a higher modal density within the bandwidth of control. So the mirror will surely be harder to control. Another issue of importance is the computer calculations. The Euro50 model will have a system order of more than 4000, which would lead to immense problems if an entire MIMO approach would be used i.e., if every position is fed back to every actuator on the mirror. This contradicts that Grocott's solution can be used on Euro50. So the control challenges of the Euro50 deformable mirror seem to be unsolved at the moment and need another solution. This fact however, does not prevent tests to see if for example a stable SISO control approach may exist. Although this thesis does not approach it more closely there may also be a future possibility to use the symmetric hexagonal shape of the mirror to reduce the system in almost the same fashion as Grocott did.

[8]The force of an actuator influences the deformation at a mirror position far away. This can be compared to the situation of a water drop falling on a calm water surface. The waves will travel over the surface until the friction makes them disappear. View the mirror as the water surface and the water drop impact as the stroke of the actuator.

2 Introduction to the Euro50 Control

The control problem and specifications of this thesis will be given in this chapter. This will be made in connection to the general control issues of the Euro50 project.

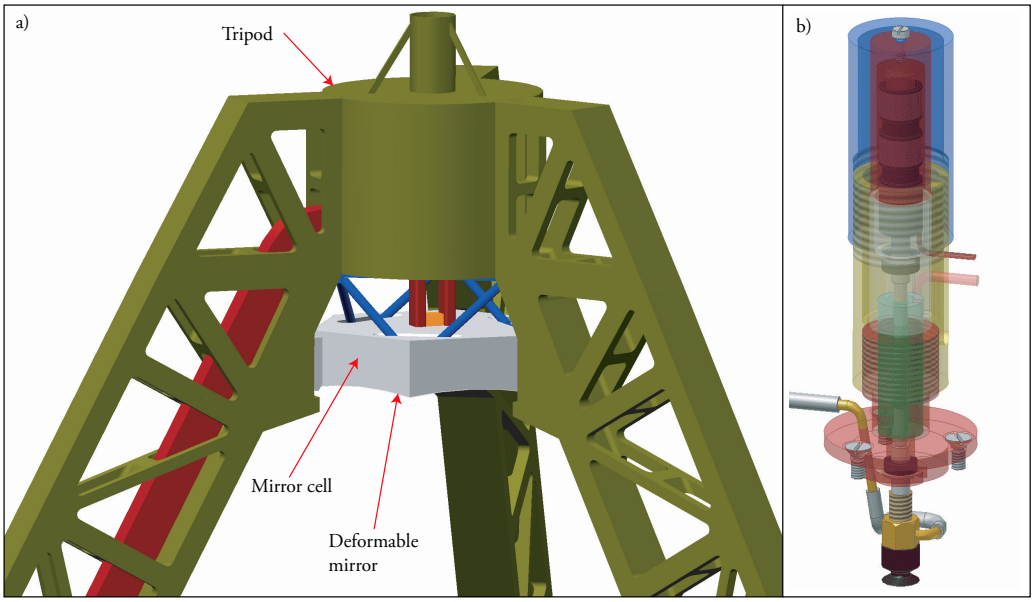

Figure 9: a) The mirror cell placed on top of the tripod (compare with Figure 1) b) The voice coil actuator, [18].

2.1 The control in general

As the modern telescopes grow bigger and bigger by every decade so does the need for sufficient control systems. The Euro50 telescope is of course no exception. Here are a few examples of what need to be controlled

- The form of the primary mirror. The Euro50 primary consists of 618 segments that must all be aligned with respect to one another.
- The shape of the secondary deformable mirror. This is the main topic of this thesis.
- The secondary mirror cell. The deformable mirror is placed underneath a rigid body cell (see Figure 9 a) that needs to have a six degree-of-

freedom control. That is, it must be kept in position when disturbed by wind loads and structural vibrations[9].

- The main servo drives and rotators. They are used to aim the whole telescope construction towards the object of observation.
- The deformable mirror actuators. Voice Coil actuators (see Figure 9 b) will be controlled[10] in order to influence the deformable mirror with the right forces, decided by the mirror shape control. They are put inside the mirror cell, just above the mirror, and will have stroke capacity up to 40 μm, measured on the mirror surface.

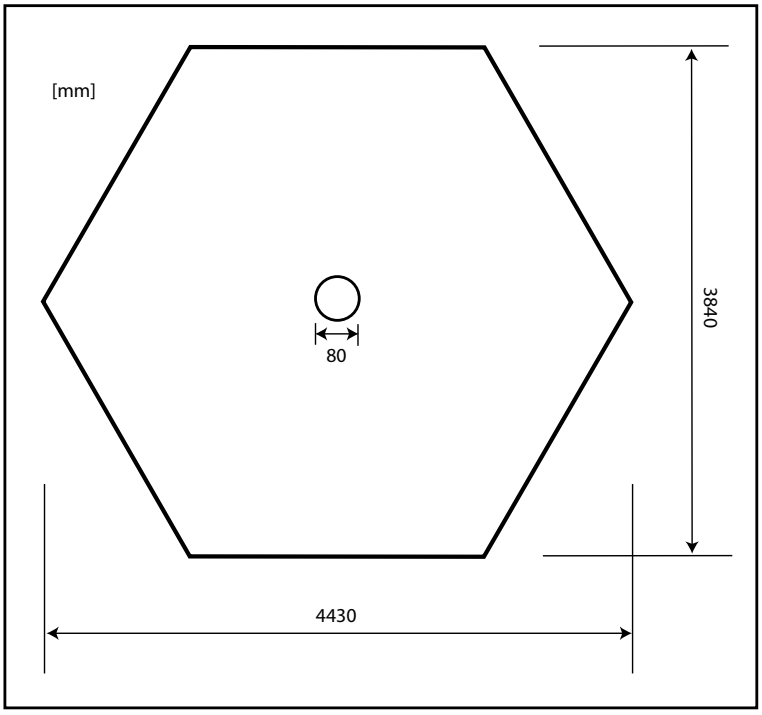

Figure 10: The dimensions of the Euro50 secondary mirror when seen from above.

2.2 The control of the deformable mirror

The purpose of this thesis is to find ways to model and control a large deformable mirror. The mirror to be used in these studies is the Euro50 sec-

[9]For more information, see [16].
[10]More information in [18].

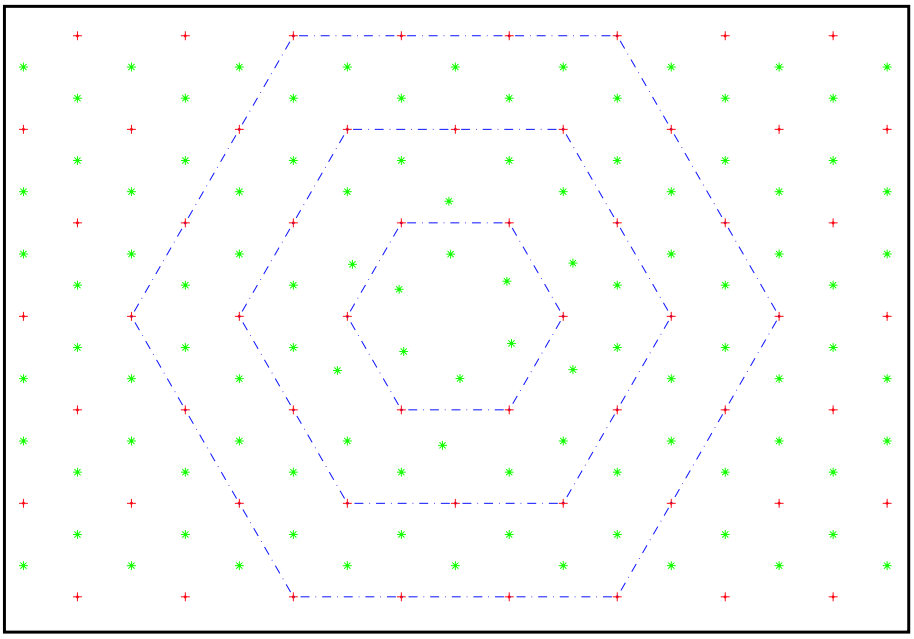

Figure 11: This is a sketch of the center of the deformable mirror. The actuators (crosses) are placed in hexagonal rings (dash dotted lines) over the mirror. Capacitive sensors (stars) are placed hexagonally around the actuators.

ondary mirror. As mentioned before it has a hexagonal shape with an equivalent diameter of four meters, see Figure 10. The mirror will have a central support with a diameter of 80 mm. The edges however will be free from additional support. To match the hexagonal shape of the mirror the voice coil actuators have been placed in hexagonal rings (see Figure 11) with a spacing of 69 mm. The first ring has six actuators, the second has twelve, the third eighteen and so on in a total of 32 rings and 3168 actuators. The center of the mirror has no actuator since it is supported there. A total of 6144 capacitive sensors are placed between the actuators like in Figure 11. These are used to measure the deformations of the mirror which is possible by the change in plate distance i.e., altering the capacitance. An alternative to this approach is to collocate the sensors with the actuators like in the MMT solution. Since this approach gives a considerably lower system order[11] it will be used here for the model and control simulations.

[11] That is, fewer computer calculations.

2.3 Thesis goals and control specifications

The first objective of this thesis is to create a state space model (i.e., a system with first order differential equations) of the deformable mirror and to verify it. The second and most important objective is to find a control law that controls the mirror.

For the Euro50 adaptive optics system to work efficiently, the mirror control will need to meet certain specifications. The fast atmospheric turbulence demands the closed loop control to have a bandwidth of at least 500 Hz. This sets a limit to the coarseness that a mirror model can have. It must have sufficient information in the frequency span of control. This can be made either by truncating frequencies above the span of control or by considering only the most important eigenmodes.

To obtain a satisfactory angular resolution of the telescope image, the maximum RMS (Root Mean Square) value of the deformation deviation allowed is 80 nm for the K-band (IR-light, 2.4 μm). In the future the telescope should also be able to operate for visual light (the V-band) as well. The maximum RMS value will then be 16 nm. The RMS-value is defined by

$$\sigma = \sqrt{\frac{1}{N}\sum_{i=1}^{N}\delta_i^2} \tag{1}$$

where N is the number of samples (e.g. time) and δ the variable, e.g. deformation, at sample i.

The RMS and bandwidth specifications are the most important for this thesis. In the future however, one will have to consider a few more areas. The maximum deformation increment from an actuator to its neighbour actuator is 2 μm. The atmospheric disturbances will not demand more of the increments. A larger value would also result in larger actuator forces than allowed.

It will also be important to consider some ranges of mirror control. Figure 12 shows these ranges. If the disturbances demand the mirror shape to bend by 20 μm then it will not have to work at maximum frequency. Small changes however mean that the frequencies of the changes may be greater and demand a control with higher bandwidth. The gray zone, in the Figure, indicates that the curve position depends on the position on the mirror. The left end point of the curve is set by

$$\delta(0) = 5 + 15\frac{r}{2} \tag{2}$$

where δ is the deformation and r is the distance from the center of the mirror.

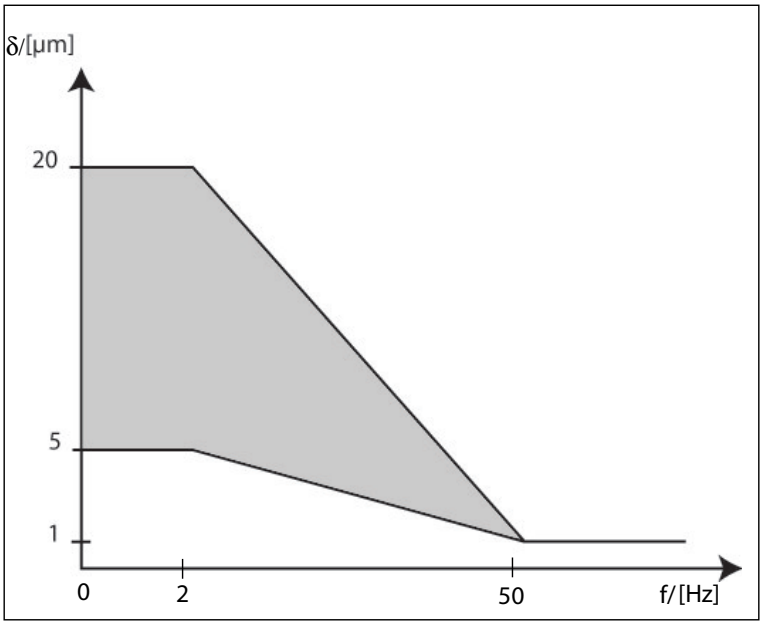

Figure 12: The dependence between necessary controller bandwidth and maximum mirror deformations needed.

3 Modeling a Deformable Mirror

The main concern of this chapter is the modeling of the deformable mirror. A modal model for the Euro50 deformable mirror will be described, derived and verified. Furthermore, a local model for a small part of the mirror will be introduced.

3.1 Theory on modal modeling

The goal of the modeling was to derive a state space model of the deformable mirror. In order to do so a standard differential equation, for flexible structures like the deformable mirror, is derived using spatial discretization and standard mechanical laws

$$M\ddot{q} + D\dot{q} + Kq = B_0 u \tag{3}$$

where M denotes a mass matrix, D is a damping matrix, K is a stiffness matrix, q is a vector of displacements, u is the system input forces and B_0 is an input coupling matrix. The system can therefore be represented by a set of masses linked by a number of springs and dampings. The system output can be viewed as a combination of displacements and displacement velocities

$$y = C_{oq}q + C_{ov}\dot{q} \tag{4}$$

where the two C-matrices are selecting the outputs used.

A state space model can be derived directly from the formulas above. It is however often an advantage if one transforms the differential equations first. The set of eigenfrequencies for the system $\omega : \{\omega_1, \omega_2, ..., \omega_n\}$ and the eigenmodes $\phi : \{\phi_1, \phi_2, ..., \phi_n\}$ corresponding to each of the frequencies can readily be obtained using for instance the Finite Element Method (FEM). In order to transform the system equations, the following matrices are defined

$$\Omega = \begin{pmatrix} \omega_1 & 0 & \dots & 0 \\ 0 & \omega_2 & \dots & 0 \\ \vdots & \vdots & \ddots & \vdots \\ 0 & 0 & \dots & \omega_n \end{pmatrix}, \quad \Phi = [\phi_1, \phi_2, ..., \phi_n]$$

The Φ-matrix is the transformation matrix and initiates the new, modal, variables q_m as

$$q = \Phi q_m \tag{5}$$

This transformation alters the system in the following way

$$\Phi^T M \Phi \ddot{q}_m + \Phi^T D \Phi \dot{q}_m + \Phi^T K \Phi q_m = \Phi^T B_0 u \tag{6}$$

$$y = C_{oq} \Phi q_m + C_{ov} \Phi \dot{q}_m \tag{7}$$

where Φ^T has been multiplied from the left in equation (6). It can be shown that

$$\Phi^T K \Phi = \Omega^2 \tag{8}$$

$$\Phi^T D \Phi = 2Z\Omega \tag{9}$$

where Z is a diagonal matrix filled with the damping coefficients ($\zeta : \{\zeta_1, \zeta_2, ..., \zeta_n\}$, known from control theory) for all modes. If the Φ-matrix is mass normalized (i.e., $\Phi^T M \Phi = I$) it holds that

$$\ddot{q}_m + 2Z\Omega \dot{q}_m + \Omega^2 q_m = \Phi^T B_0 u \tag{10}$$

This is the *modal model* of flexible structures which can be applied to the deformable mirror. The modal state space form can be derived by transforming the second order equations into a set of first order equations, introducing the new state variables $x = (x_1, x_2)^T = (q_m, \dot{q}_m)^T$. This gives

$$\dot{x} = Ax + Bu = \begin{pmatrix} 0 & I \\ -\Omega^2 & -2Z\Omega \end{pmatrix} x + \begin{pmatrix} 0 \\ \Phi^T B_0 \end{pmatrix} u \tag{11}$$

$$y = Cx + Du = \begin{pmatrix} C_{oq}\Phi & C_{ov}\Phi \end{pmatrix} x \tag{12}$$

The system is a combination of n second order systems whose characteristics are well known from control theory. The main advantage of this system in comparison to the one containing the M-, D- and K-matrices is that the individual modes are decoupled so the model matrices hold many zeros. This enables the use of sparse matrices in Matlab and Simulink, decreasing the number of calculations needed.

For those who would like to know more about modal models, read for instance [10] and [11].

3.1.1 The 2002 modal model

The 2002 lowest Euro50 deformable mirror eigenfrequencies (up to 1165 Hz) and their respective modes were collected from a FEM model, developed at Lund Observatory. Since the CFRP material has low damping, all ζ-values were set to 0.02, which is an approximate number. This means that the modal damping matrix becomes $Z = 0.02I$ and the system matrix is then completely determined (I is the identity matrix). Since the input vector u corresponds to all actuators, the B-matrix has as many rows as there are actuators (i.e., 3168). Given that all actuators are used B_0 is a 3168×3168 identity matrix. This gives the following B-matrix

$$B = \begin{pmatrix} 0 \\ \Phi^T \end{pmatrix} \tag{13}$$

The C-matrix is derived in almost the same fashion. Since the displacement velocities stay unmeasured and all displacements are measured by capacitive sensors, $C_{ov} = 0$ and $C_{oq} = I$. Therefore the C-matrix becomes

$$C = \begin{pmatrix} \Phi & 0 \end{pmatrix} \tag{14}$$

Since it has not yet been decided where to place the displacement sensors for the Euro50 mirror, a few different models have been derived for the cases when

1. 6144 sensors are placed between the actuators as in Figure 11,
2. 3168 sensors are collocated with the actuators,
3. 6144 plus 3168 sensors are placed between and on the actuators,
4. 6144 plus 3168 sensors are placed between and on the actuators plus 192 extra sensors which are put on the edge of the mirror.

Each case gives a different C-matrix. The other matrices, however, remain unaltered. Since the bandwidth of the controlled mirror needs to be at a frequency of about 500 Hz, each of the models above were truncated. Case number two was the model used for control purposes in this thesis. The other cases give models of very high order which are cumbersome to simulate and they were therefore not used.

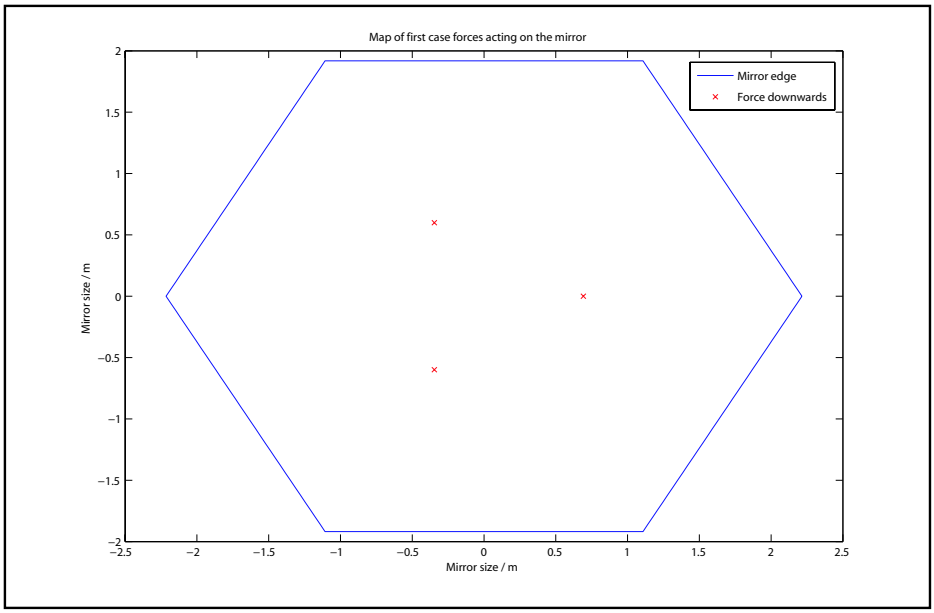

Figure 13: Test case 1

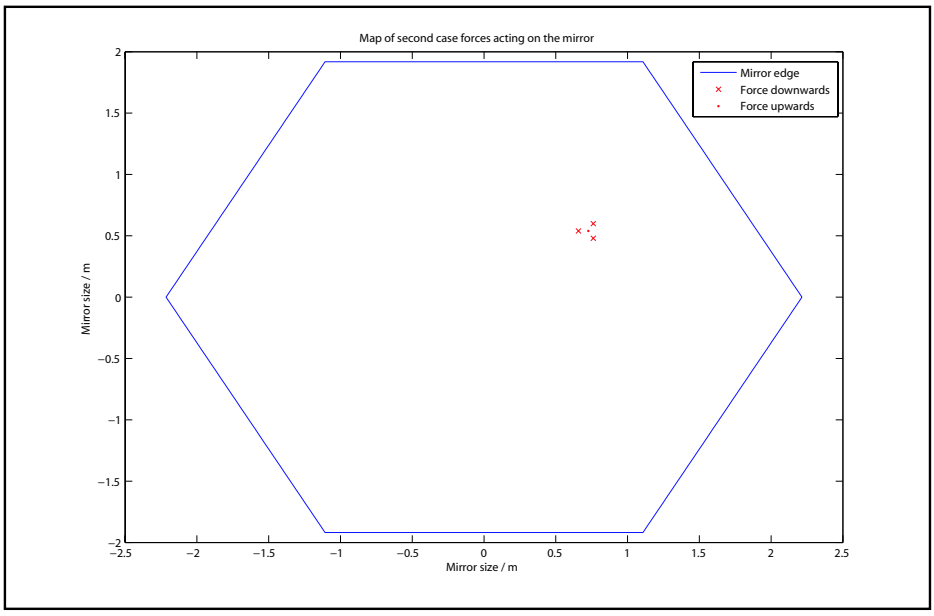

Figure 14: Test case 2

3.2 Verification of the mirror model

In order to verify the modal model it was compared with the full FEM model. Since the modal model is basically a truncated version of the FEM model, the hope was that the two models would give almost the same outputs when disrupted by forces. To ensure that this was the case, two scenarios were tested. The first scenario has three isolated forces (each of $-10N$) placed in a symmetric pattern around the center of the mirror, see Figure 13. In the second test case, four forces are influencing the mirror surface. One actuator ($+3N$) and three of its nearest neighbour actuators (each $-1N$) are operating, see Figure 14.

Due to time consuming calculations, the FEM model was not used for a dynamic verification. The static mirror deformations, for each case, using the FEM model were available however. So the model verification was based on the static case alone. The static gain of the modal model was derived using the transfer function when $s = 0$, i.e.

$$G(0) = -CA^{-1}B \tag{15}$$

Now, the static gain multiplied by the force vector becomes the static displacements of the mirror. That is

$$y(t = \infty) = -CA^{-1}BF \tag{16}$$

Where F is a constant force vector, corresponding to the actuators. This makes a comparison of the models possible.

The static deformations of the first test case, using the 2002 modes modal model, is shown in Figure 15. Note that for the deformations to be visible, the scalings of the axes are not equal. In order to compare these results with the deformations of the finite element model the residuals were inspected, see Figure 16 and the code in Appendix A.2. The Figure shows that the residuals are greater at three isolated points, corresponding to the three operating actuators. The largest error is 9.38 μm while the average error is 88 nm. Therefore the residuals outside the neighbourhood of an operating actuator are neglected. To further confirm this line of reasoning a contour plot was made, see Figure 17. As expected, the residuals seem to be correlated in the local areas of the operating actuators alone. In Figure 18, the position for one of the three test actuators has been zoomed upon. The valleys in Figure 16 are right above the three force giving actuators and the small peaks around the top correspond to the six neighbour actuator positions, i.e. about

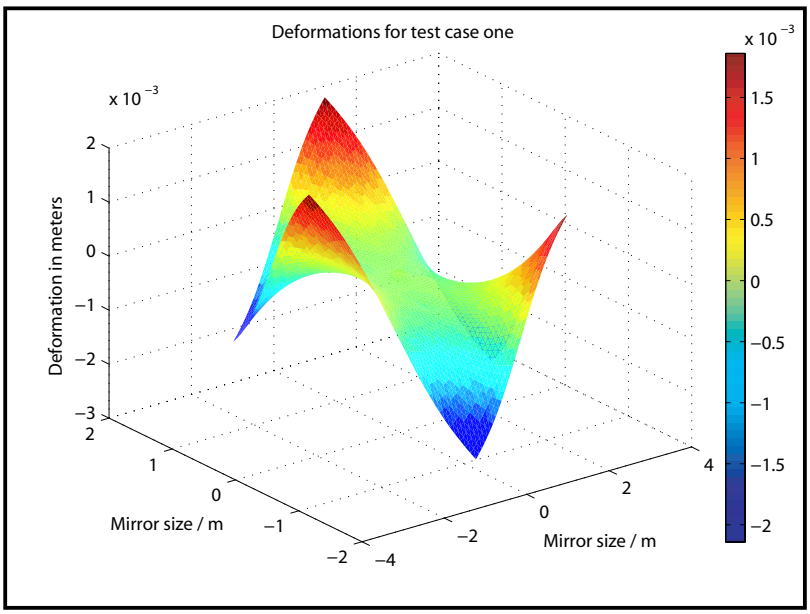

Figure 15: Static mirror deformations for test case 1 using the 2002 mode model.

6 cm away from the operating actuator. So the modal model is obviously at its worst up close to the force giving actuators, at least when the forces are isolated as in case 1. To see the relative error of the modal model compared to the FEM model, a slice of the deformed mirror was plotted in Figure 19. This is a good measure of the model reliability and it shows that the error ratio is about 1.18, i.e. the difference is about 18 %. So even though the model error residuals are rather large compared to the specifications of the mirror control, the model may still be rather reliable statically.

The second test scenario shows a case where the coupling between neighbouring actuators becomes evident. The same plots as for test case 1 could have been reviewed, but the most interesting part is the analysis of the model residuals as can be viewed in Figures 17-19. The case 2 contour plot and a zoom in on the operating actuators can be viewed in Figures 20 and 21. The largest errors seem once again to be located at the four operating actuators and they are all at about 1 μm as in test case 1. The slice plot in Figure 22, that covers two actuators (one up and one down), shows that the relative errors are greater in this case than in the previous. The relative error at the $+3N$ actuator is for example 39 %, while it is even greater at the other three actuators. This is the result of the static coupling between the four actuators. The coupling of the local actuators have thus made the relative

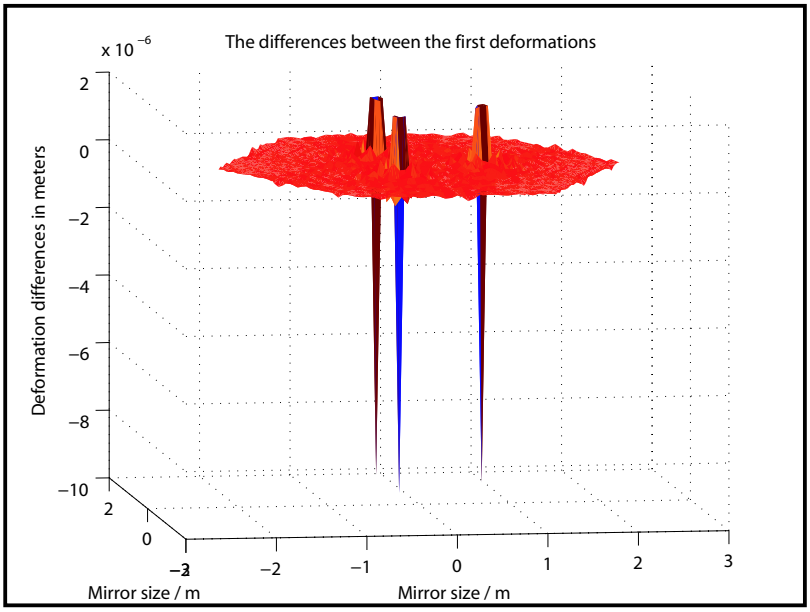

Figure 16: Deformation residuals between the FEM model and the modal model, test case 1.

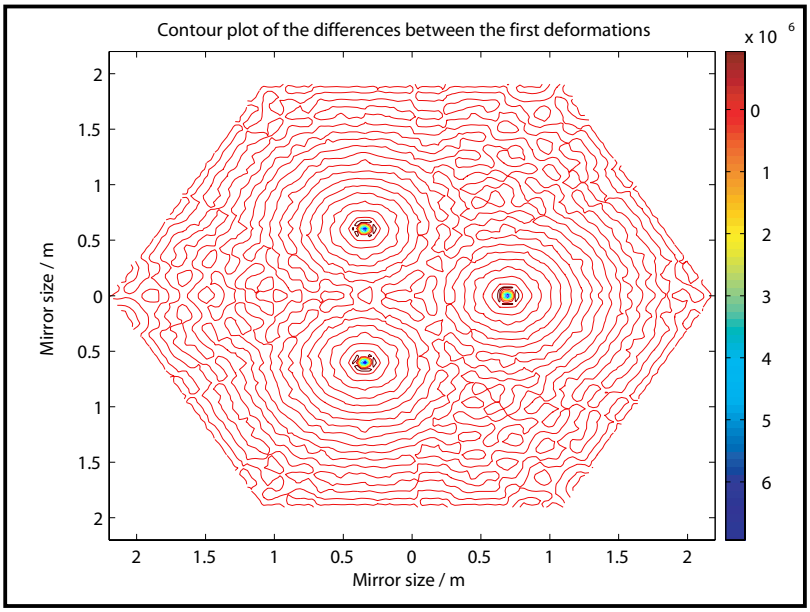

Figure 17: Contour plot of the residuals in test case 1.

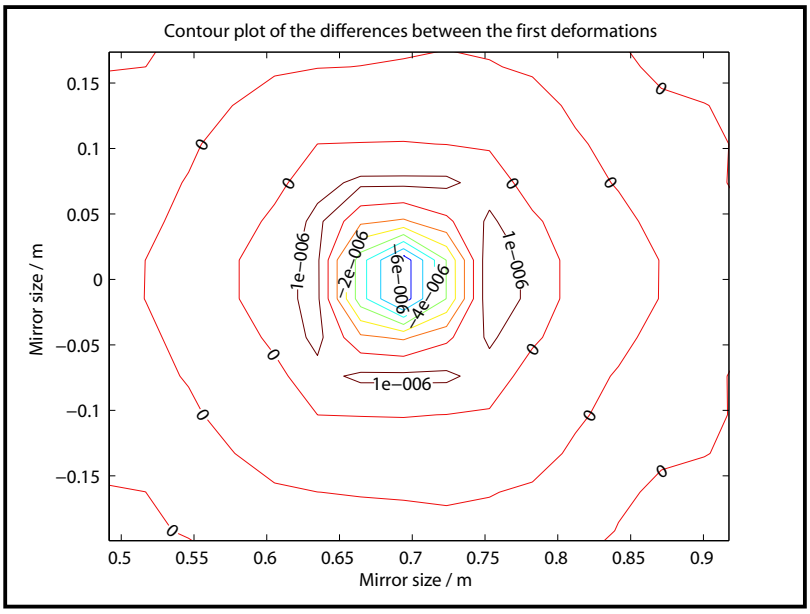

Figure 18: A zoom of the contour plot at the position of an operating actuator. The zeros comes from the fact that the resolution of values in the contour plot is not good enough.

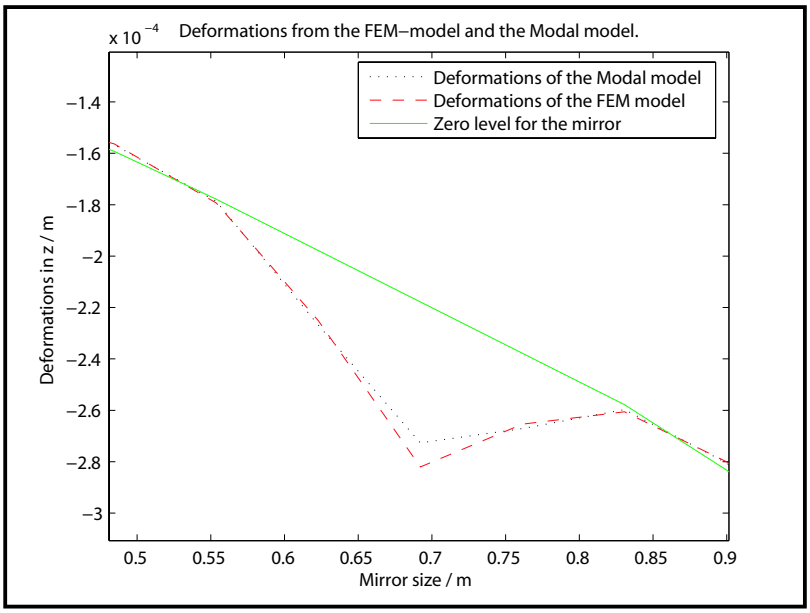

Figure 19: A slice of the mirror deformations in test case 1 (compare with Figure 15) close to one of the operating actuators using the modal model and the FEM model.

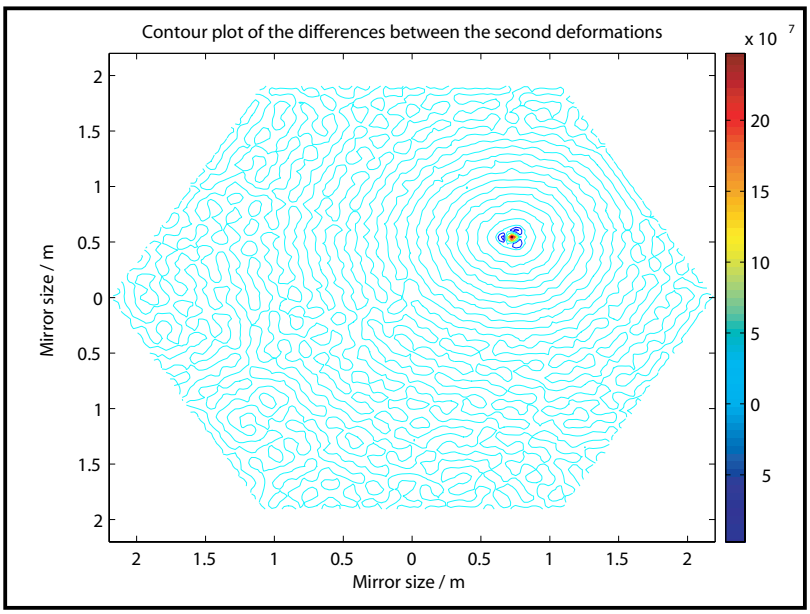

Figure 20: Contour plot of the residuals, between the modal and FEM models, in test case 2.

errors more significant.

Why are the two mirror models not identical? The modal model is derived directly from the FEM model, but the complete FEM model many more than 2002 modes. All the necessary information is therefore not available. The modal model is also based only on the modal values at the sensors and the actuators and this does also contribute to the total error.

The question now is whether the modal model is relevant and if so, can one reduce the model even further in some fashion, through direct truncation or something else?

Although a dynamical verification was impossible, the 2002 modes modal model was still simulated to see if the models behaved as expected. The final values seemed to be correct for all values looked upon.

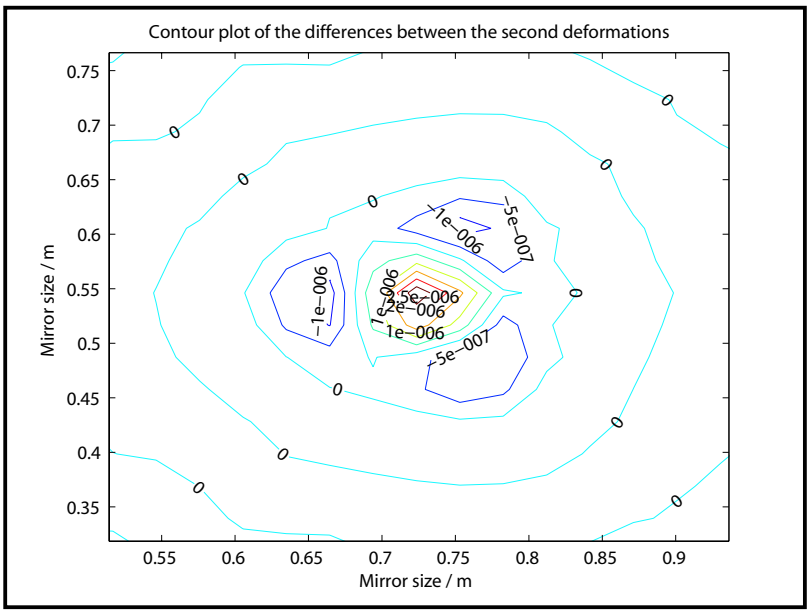

Figure 21: A zoom of the contour plot at the position of the operating actuators.

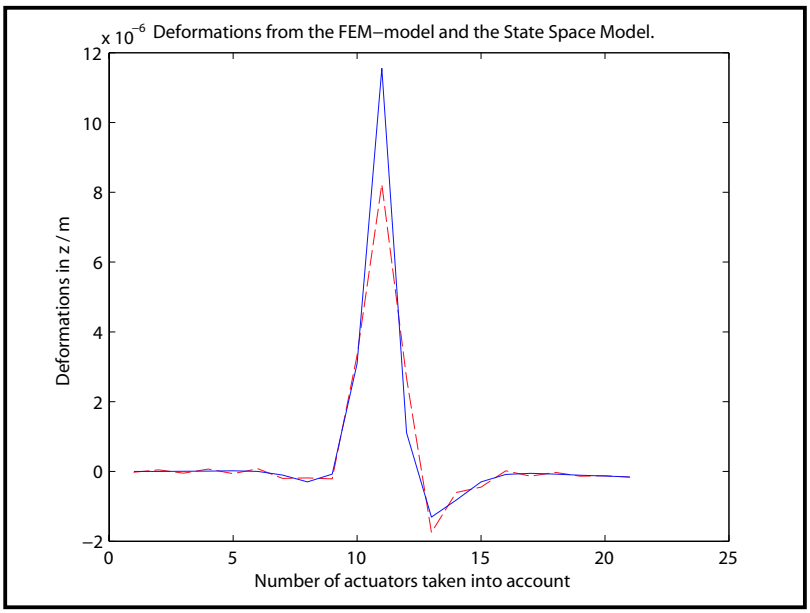

Figure 22: A slice of the mirror deformations in test case 2 close to the operating actuators showing two of these at position 11 and 12. The dashed line corresponds to the 2002 mode model and the full line features the FEM model.

3.3 Other mirror models

3.3.1 A Guyan reduced mirror model

Since the full finite element model was too big to be used in Matlab simulations, a truncated 2002 mode version was used. This model however had quite large static errors as was described in the past section. To improve the model used, one can start over and reduce the full FEM model using another principle than modal truncation. This was done by Torben Andersen and Holger Riewaldt [5] at Lund Observatory. The reduction method used was the so-called Guyan reduction. This approach allows a selection of the most important degrees of freedom (dof) in the full mirror model. The idea is that these dofs have larger influence on the dynamic behaviour of the mirror. The full model had 445696 dofs and the reduced one has 3354 dofs.

The new model was implemented as a modal model, with order 6708, similar to the 2002 mode model. A static verification between this model and the FEM model, i.e. test cases 1 and 2, showed a much better match than the 2002 mode model. The eigenfrequencies of the new model are however somewhat higher. The first 800 eigenfrequencies are approximately 1 percent higher than for the full model. The relationship grows to 2 percents for the next 100 eigenmodes and increases further. The accuracy however, seems to be sufficient within the range of control (i.e. up to 500 Hz).

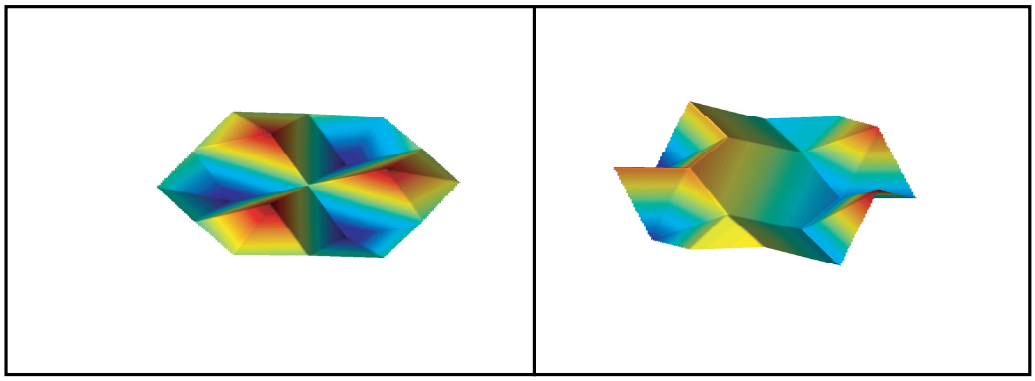

Figure 23: Two local mirror eigenmodes.

3.3.2 A local mirror model

The full models have several thousand states which make them difficult to use when designing a control system. Cumbersome calculations and numeri-

cal problems tend to put limits to the analysis of the process. A solution to this problem is to divide the full model into many small models. The idea is to create sections of the mirror with 19 actuators in each local model. The local models are derived using the Guyan reduction method once again on the previous Guyan reduced model[12]. This was done by Torben Andersen[13] at Lund Observatory in connection to this thesis. Just like the full model, the local model will have a number of eigenmodes. The model contains 19 eigenmodes and is of modal state space type. Two of the eigenmodes can be viewed in Figure 23. Since the mirror dynamics change depending on where on the mirror surface the local model is placed, many local models will have to be considered overlapping each other.

The local model is of order 38 and is much easier to work with than the full mirror model. This simplifies the control design a great deal and opens up for a MIMO controller approach.

[12]For more information on how to create local models please read [17].

[13]In a text about the reductions, Torben Andersen explains why Guyan reduction can be applied once again: "Although use of Guyan reduction to go from a system with 6708 degrees of freedom to 38 degrees of freedom is somewhat questionable, it seems acceptable in this case because the higher frequency modes that characterize the local system are likely to be correctly modeled. The low frequency modes that are not modeled adequately are not likely to play a large role for the local control system because they largely mimic rigid body motion."

4 The Control of a Large Deformable Mirror

In the process of this master thesis several different control strategies have been investigated. Single Input Single Output (SISO) control was the first technique to be used and is described in this section. In the modeling verification section, 3.2, difficulties with heavy cross couplings between controlling actuators was brought to surface and may make SISO control inadequate in reality. The control is therefore expanded trying to handle this predicament where the force of an actuator generates waves on the surface of the mirror. At first, however, basic control theory and ways to ensure sufficient robustness are discussed.

4.1 Stability and robustness

4.1.1 Phase margin

It is often not enough that stability is ascertained, but it is also important that certain margins to stability are met. Analysing the phase margin is one method developed for identification of system robustness.

Stability margins are important since they permit the process to vary within certain limits. This is significant when taking model deviations and time delays into account. The margins are also putting limits to the performance of the control loop. Too large stability margins may result in slow control, while undersized margins give poorly damped and uneasy control.

The phase margin is often denoted ϕ_m and is a measurement of how much the phase can decrease before the system becomes unstable. The phase margin can be displayed in a Bode diagram, Figure 24, where it is the value between -180 degrees and the phase curve at the cut-off frequency, ω_c, which is determined by

$$|G_0(i\omega_c)| = 1 \tag{17}$$

The phase margin is then

$$\phi_m = \pi + arg G_0(i\omega_c) \tag{18}$$

A phase margin within the region of 45^o to 60^o is a rule of thumb for good control ([13]).

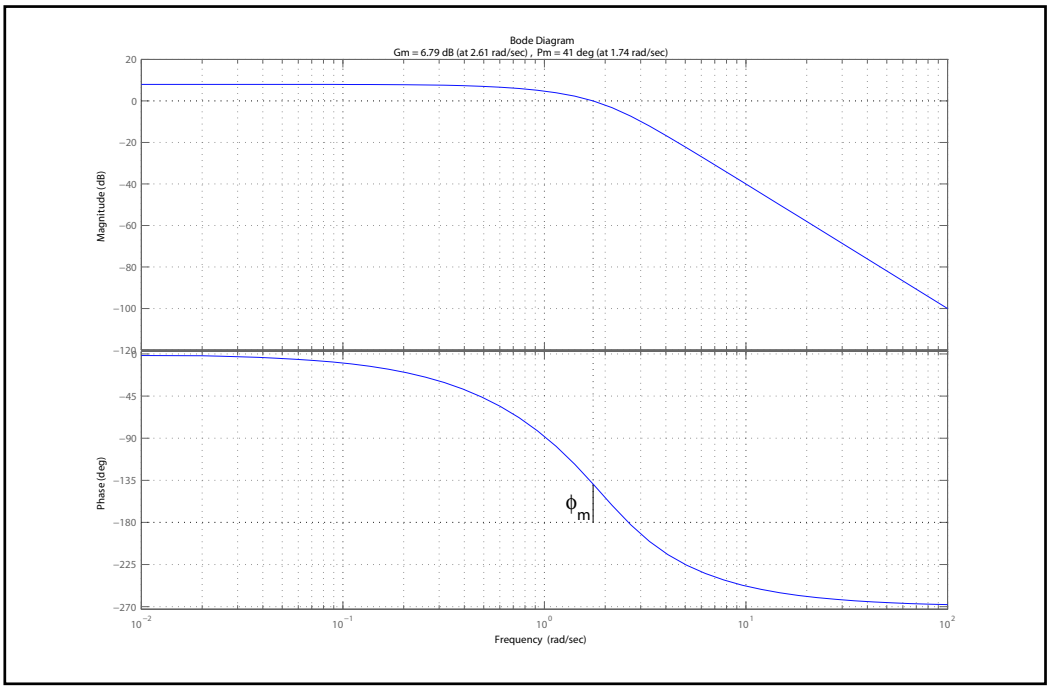

Figure 24: Bode diagram displaying the phase margin which is 41 degrees.

4.2 System compensations

In order to define the closed loop characteristics for a system, the open loop is often analysed and modified using e.g. Bode diagrams ([13]). Three different compensation filters are discussed in this section, all of which manipulate the system in either giving it a higher bandwidth, higher static gain or ascertaining its robustness, i.e. making stability margins large enough. The three filters are phase lag, phase lead and band pass filters.

4.2.1 Lag filters

Lag filters are designed with the purpose of increasing the low frequency gain. The phase however, is decreased in a certain frequency range. These two effects can be seen in Figure 25. The main benefit of the filter is that the increased low frequency gain results in a smaller stationary error. The drawback is that the phase decrease might lead to a smaller bandwidth. The lag filter has the transfer function

$$G(s) = \frac{s+a}{s+a/M} \qquad M > 1 \tag{19}$$

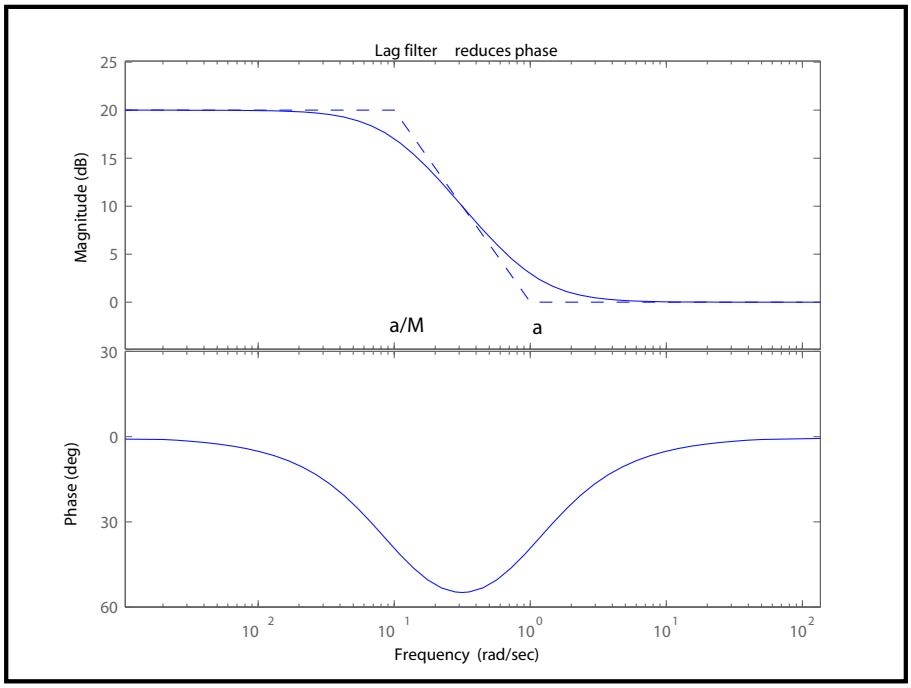

Figure 25: Bode plot of a lag filter. The dashed line displays the asymptotes.

Since the parameter M is greater than one, the first break frequency comes at a/M rad/s and the second at a rad/s. The a-value is chosen so that the phase at a certain frequency, ω, is not decreased too much. In general, ω is the cut-off frequency, but since the Bode plots of the mirror system might have many cut-off frequencies it has been chosen with more care throughout this thesis. A rule of thumb is to choose $a = 0.1\omega$, which ascertains a maximum phase decrease of 6 degrees at ω. A high factor M gives a low stationary error since it is also the static gain of the lag filter.

4.2.2 Lead filters

Lead filters are designed to increase both phase and magnitude at the cut-off frequency, see Figure 26. The transfer function for lead filters is of the form

$$G(s) = KN\frac{s+b}{s+bN} \tag{20}$$

A zero at frequency b rad/s forces the phase to increase and a pole breaks it down at bN rad/s ($N > 1$), see Figure 26. The maximum phase gain that can be achieved is $+90^o$. As was mentioned, lead filters are often used

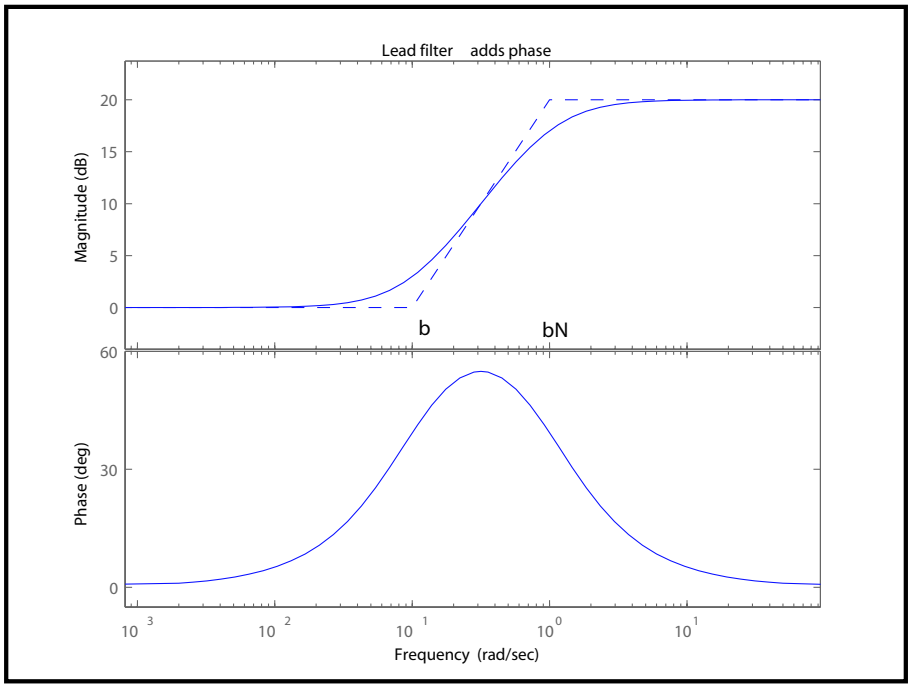

Figure 26: Bode plot of a lead filter. The dashed line displays the asymptotes.

to increase the phase around the cut-off frequency, but introducing a lead filter also increases the gain at higher frequencies. This is a quality that is sometimes hard to deal with if there is high frequency noise in the process.

4.2.3 Band pass filters

A band pass filter is used to increase the gain for some frequencies ([15]). As models and reality do not match in all characteristics, it can be dangerous to cancel poles at specific frequencies and therefore a wider bandpass filter is used containing multiple inverted Notch filters lying next to each other. The transfer function for an inverted Notch filter is

$$G(s) = \frac{s + \omega^2}{s^2 + 2\zeta\omega s + \omega^2} \tag{21}$$

View Figure 27, which shows the Bode plot for such a filter. In order to achieve a nice round bandpass filter, the damping, ζ, must not be chosen too small. This should, however, be weighed by the fact that a damping coefficient close to 1 gives a low gain increase and the positive effects of the filter are thereby gone.

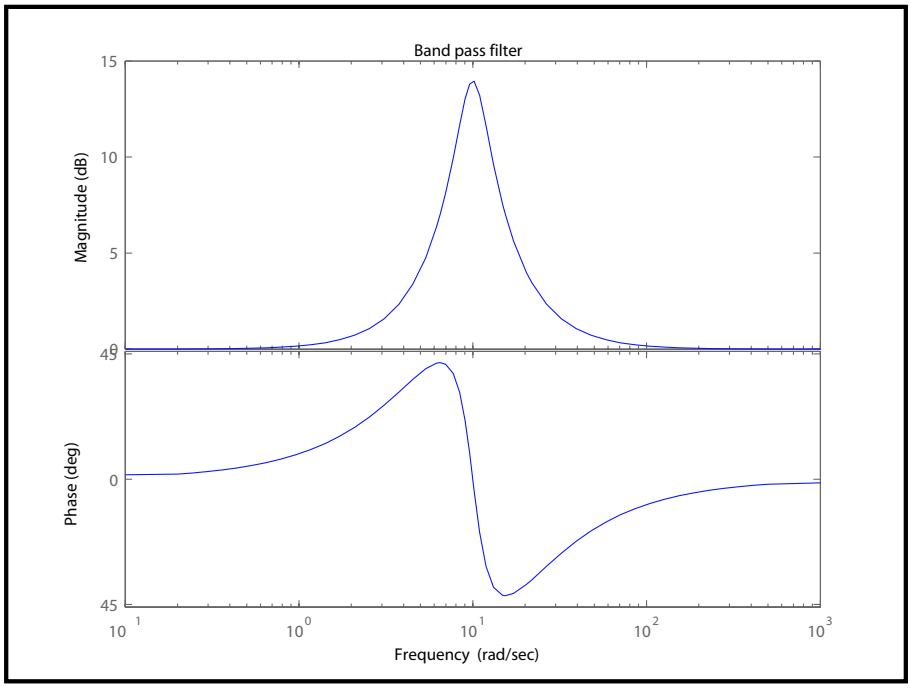

Figure 27: The Bode plot for an inverted Notch filter.

4.3 SISO control of the deformable mirror

4.3.1 Transfer functions for the individual actuators

It seems reasonable that the hexagonal symmetry of the secondary mirror would affect the transfer functions. A verification of this shows that transfer functions from actuator forces to their deformation outputs are equivalent for actuators in the same hexagonal rings. It was therefore decided to study the actuator transfer functions located on a straight line from the center of the mirror to the edge, as displayed in Figure 28. In this way, the actuators could be put together in families according to the relative distance to the center of the mirror. Each family can then be controlled using only one controller. The system transfer functions were composed by the script in Appendix A.3 and the Bode plots (from the actuators' forces to their deformations, i.e. SISO systems) for all systems on the straight line can be viewed in Figure 29. Those actuators with similar transfer functions were placed in the same family and a total of six families were used.

Examining Figure 29, one can conclude that the actuators with shortest distance to the center of the mirror are the ones with the lowest static gain

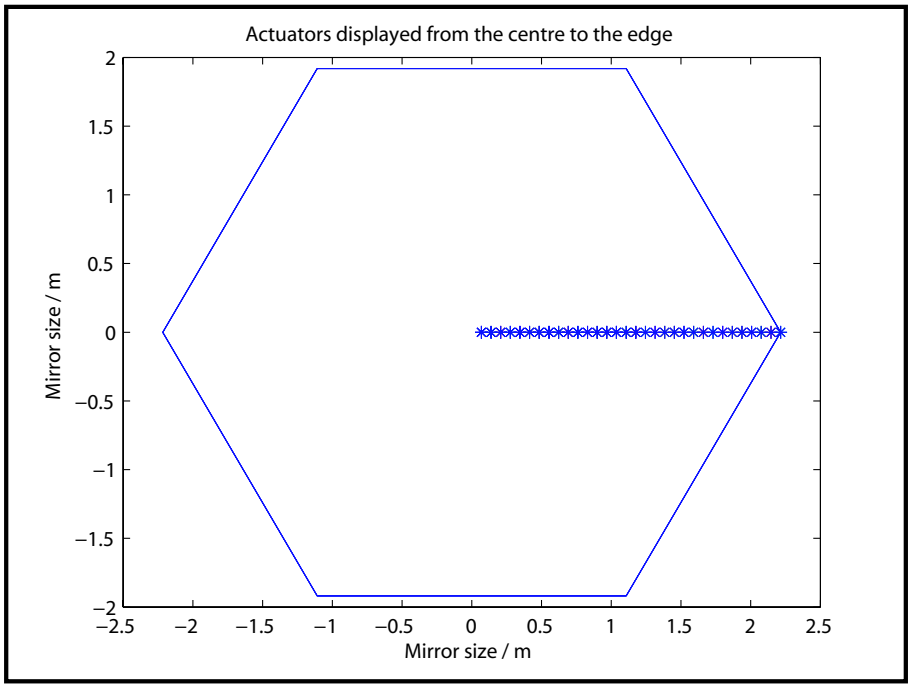

Figure 28: The actuators from the center of the mirror to the edge.

and the ones with highest static gain are the ones placed at the edge of the mirror. This comes from the nature of the system, in which the mirror is attached to the mirror cell at its center only. This results in low static gains at the center and large static gains at the edge, caused by the greater torque implied by the actuators at the outer limit of the mirror.

4.3.2 SISO control using compensation filters

As it would be impossible to meet bandwidth and root mean square specifications using only one control loop, the transfer functions were placed into families depending on their characteristics, see Figure 29. SISO control loops were then developed using compensation filters, mostly lead and lag filters. Band pass filters were used to a smaller extent as troubles with deep gain losses for relatively low frequencies only occurs at some actuator locations. This characteristic can be viewed in Figure 30 at frequencies 30 rad/s and 100 rad/s.

Refer to the uncompensated SISO system in Figure 30, i.e. one of the functions from Figure 29. To meet the bandwidth specification of 500 Hz, it is

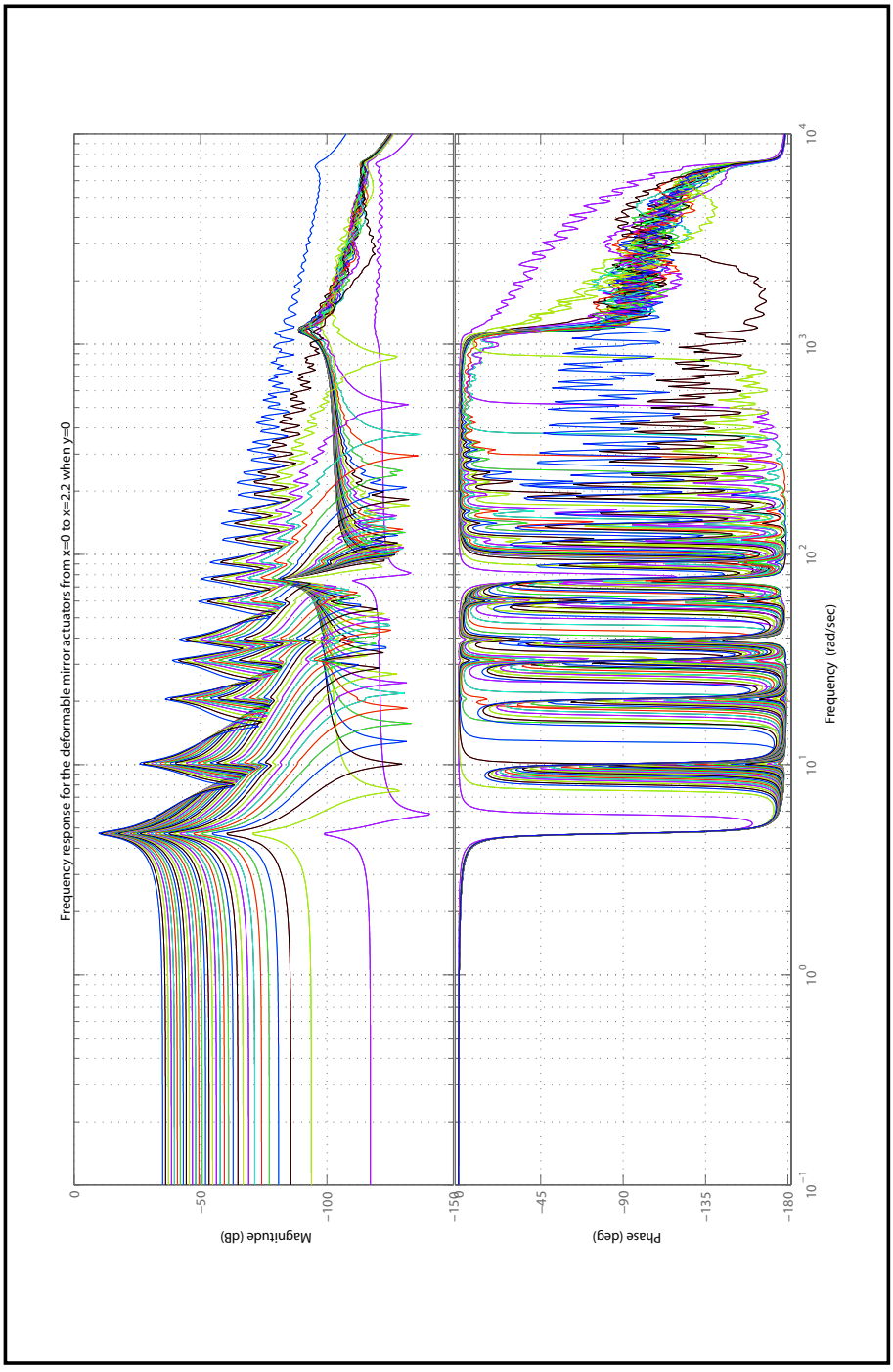

Figure 29: The transfer functions, from actuator force to deformation at the same actuator position, for all 32 actuators in Figure 28.

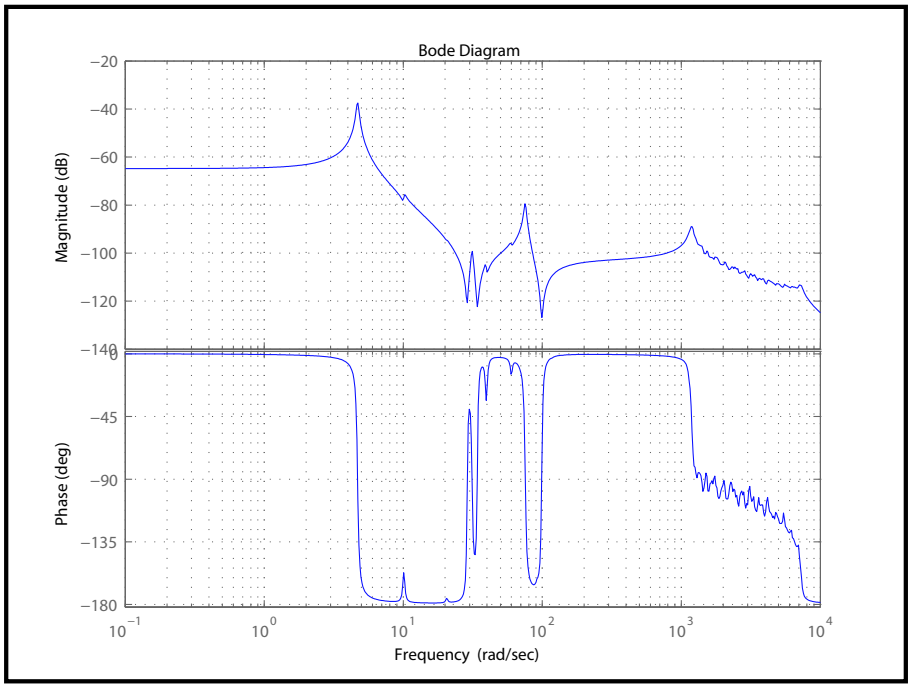

Figure 30: One of the uncompensated transfer functions displayed in a Bode diagram.

necessary to place a band pass filter over the deep valleys in the gain plot. It may also be desirable to enhance the low frequency gain, which is done by placing a lag filter for these frequencies. As the phase is close to zero at these frequencies there will be no risk of turning the system unstable. At last a lead filter is placed to increase the phase margin for frequencies where the phase is dangerously close to -180^o. The compensated system is displayed in Figure 31. The full line represents the compensated transfer function and the dotted line demonstrates the compensation link.

4.3.3 Results of the individual control

The control loop families were tuned to meet the specifications and a step response test was used to validate the quality of the control. When the control loops had been designed they were tested on their separate SISO systems using a reference signal more representative for real telescope control[14]. A block diagram for the test configuration is displayed in Figure 32.

[14]The realistic control signals have been produced by adaptive optics scientists in the Euro50 project group.

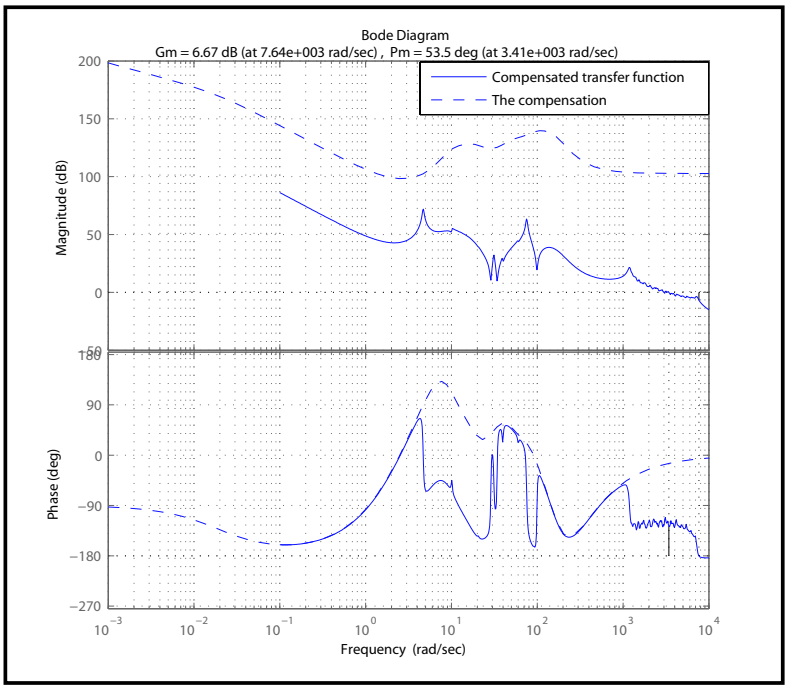

Figure 31: Compensated transfer function displayed in a Bode diagram.

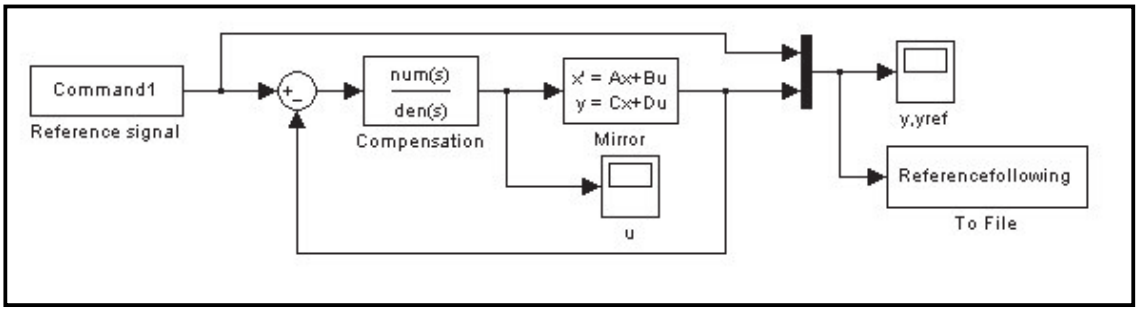

Figure 32: Simulink block diagram used when realistic references were tested.

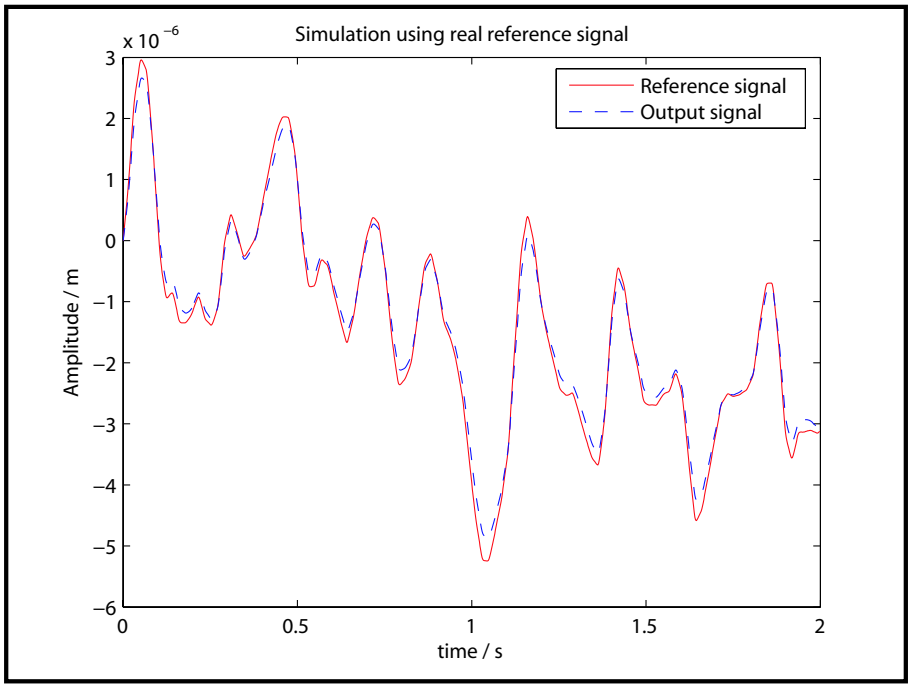

Figure 33: Reference and output signal from the block diagram in Figure 32.

From the scope in Figure 32, it can be seen how well the reference signal is tracked, see Figure 33. This control, however, does not say anything about the performance on the full mirror. It is just an indication of how every family would behave without any cross couplings in the full system. It can be seen in the Figure that the reference is tracked, but it is hard to tell how large the relative errors are by just looking at the Figure. The root mean square value (RMS, see Equation 1 in Section 2.3) for the residuals (reference minus output) were calculated to 190 nm for one of the worst performing control loops and 16 nm for one of the best. The quality of the control depends on how well the SISO controller is designed for the family member experimented on. The specifications were clearly not achieved for every actuator position on the mirror. The question is now whether or not it is possible to stabilize the full mirror system.

4.3.4 SISO control of the full mirror

Experiments on the mirror showed that the system was unstable when the SISO families were used. The first guess was that the cross coupling effect caused the trouble. In order to determine the source of instability, fewer and

fewer actuators were used to control the mirror[15]. As assumed, a sparse grid of actuators resulted in a stable system, while a dense grid caused instability. This supports the assumption of the cross coupling difficulty. As mentioned before, the coupling effect may be viewed as waves generated by a stone falling into a calm pool of water. The generated mirror waves need to be suppressed, but how?

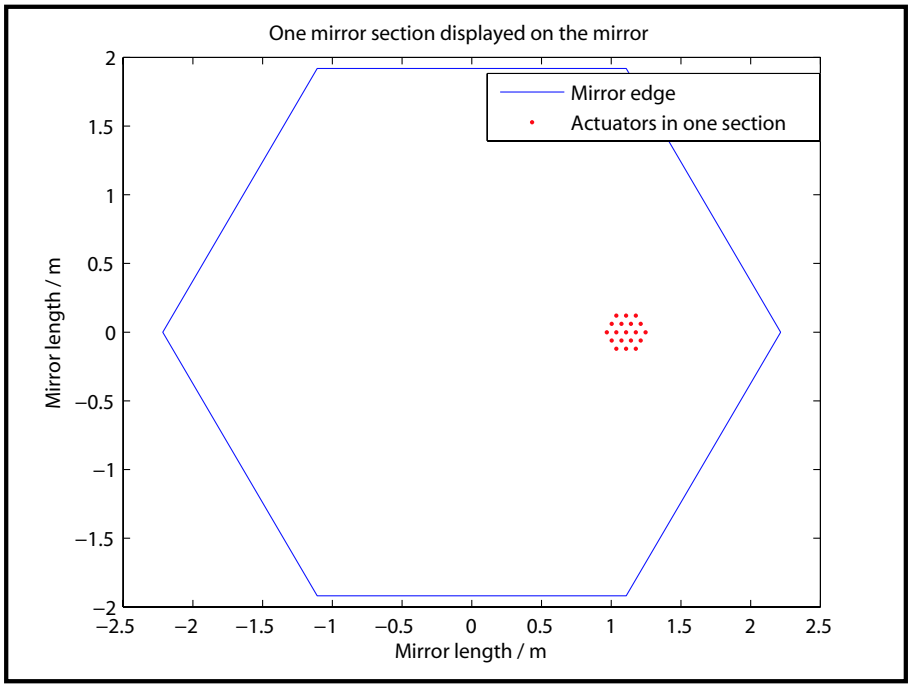

Figure 34: The dots indicates the local mirror section. The center actuator is the actuator actively controlled. A static force distribution is then applied to the two hexagonal rings next to the actuator.

4.4 Local control using a static force distribution

4.4.1 Strategy of local control

In order to suppress cross coupling effects on the mirror surface, a local model of the full mirror (see Section 3.3.2) was used. The model contains 19 actuators (see Figure 34) where the actuator in the center is controlled by a compensation link. The idea of the local control is to place forces, in two

[15]The case with only one actuator corresponds to the individual control in the previous section.

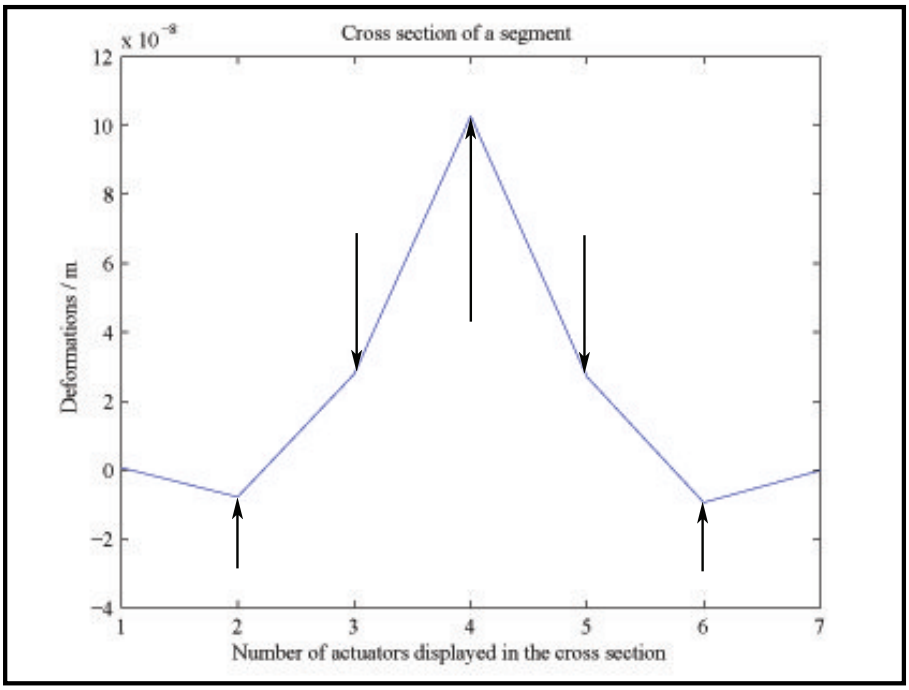

Figure 35: Cross section of a local model describing how the static forces are applied.

neighbouring hexagonal rings around the active center actuator, that will counteract cross-coupling deformations. The purpose of the force distribution is shown in Figure 35. The Figure is a slice of a local mirror model with the active center actuator displayed as number four. Actuator number three and five represents the closest neighbours while actuators two and six are situated in the second hexagonal ring.

Ideally, the center actuator force should not affect the deformations at the other actuator positions. This however is impossible, so the goal is instead to have as small deviations as possible. The most straight-forward strategy would be to generate all forces dynamically. Due to the complexity of the system, however, the first approach was to apply the force distribution mentioned above. This distribution is produced from the transfer function matrix[16] of the local state space model and should set the neighbouring deformations to zero statically. The transfer function matrix $G(s)$ can be derived from the state space matrices of the local model.

$$G(s) = C(sI - A)^{-1}B \tag{22}$$

[16]Functions from actuator forces to deformations at the actuator positions.

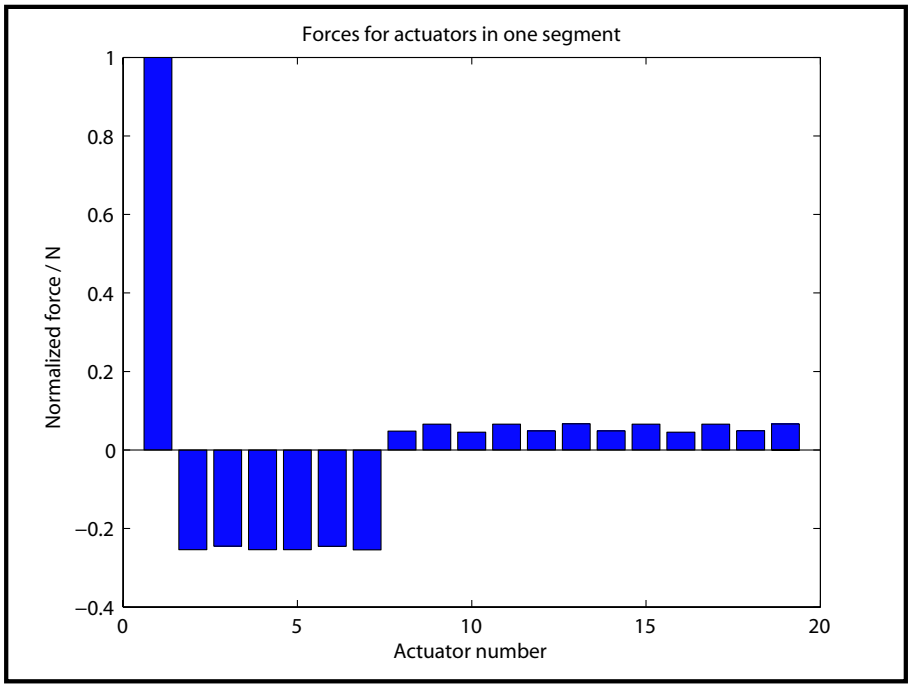

Figure 36: The normalized force distribution of a local model. Number one is the active center actuator, two to seven are the actuators in ring one and eight to nineteen are the actuators in ring two.

Here, I is the identity matrix and s should now equal zero since manipulations of the deformations were constrained to static forces alone[17]. Now

$$G(0) = -CA^{-1}B \tag{23}$$

$$Y(0) = I_1 = G(0)F(0) \Rightarrow F = F(0) = (G(0)^{-1}I_1) \tag{24}$$

$Y(0) = I_1$, i.e. the first column in the identity matrix, because this is the desired static deformation output, with the center actuator output set to one while the rest remains uneffected. Since the distribution should not affect the central force, the force distribution F is normalized

$$F = (G(0)^{-1}I_1)(I_1^T G(0)^{-1}I_1)^{-1} \tag{25}$$

The normalized forces are displayed in Figure 36. F can then be used in the control by multiplying it with the force coming from the center actuator. The result is a vector with 19 inputs which are fed into the local model.

[17]The static case is represented by zero frequency.

4.4.2 Results of the local control

Before taking the local control onto the full mirror, transfer functions for local models at different locations on the mirror were examined. It was found that local models in the middle, close to the edge and close to the center of the mirror all behaved almost equally when effected by their respective force distribution (see Figure 37). Only one compensation link was therefore needed for loop shaping. So, the control system was stable independent of which local model[18] the controller was tested on. Therefore, the coupling effects seemed less important and the control was applied to the full mirror system.

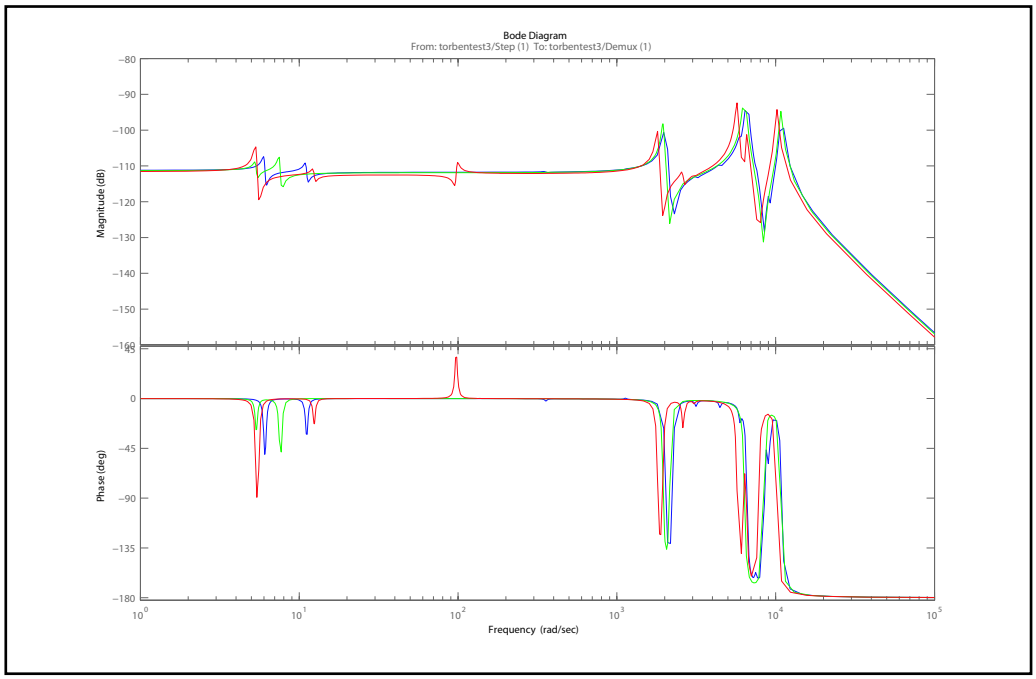

Figure 37: The transfer functions from the middle actuator force to its deformation for different positions on the mirror. The blue line correspond to an actuator close to the center, the red close to the edge and the green one from in between.

4.5 Local control of the full mirror model

The local control was implemented on the full mirror and it was impossible to achieve a robust control with only one active local section. The deformation

[18]Several local models were derived corresponding to different mirror positions.

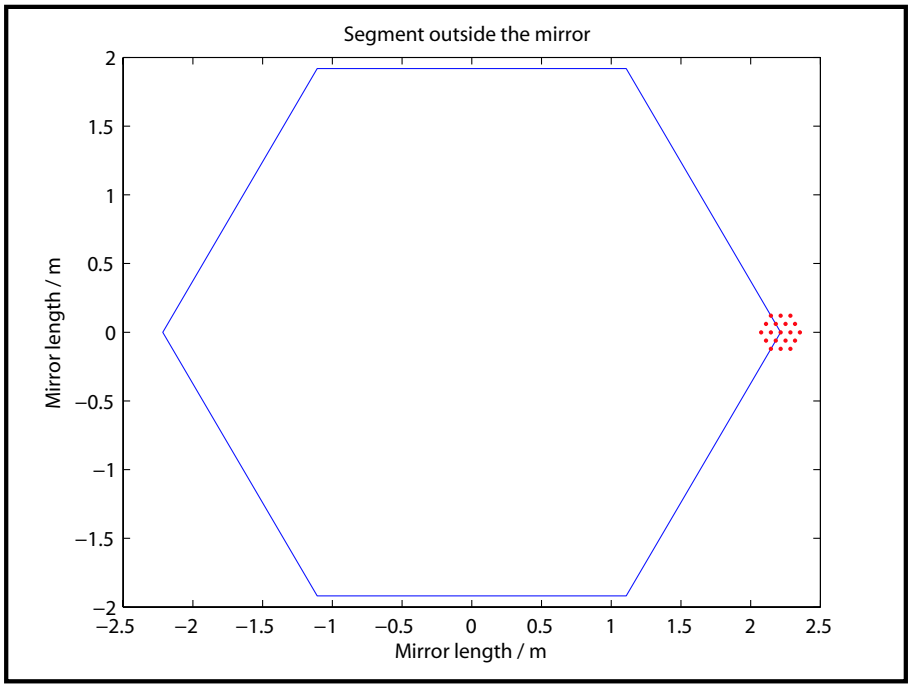

Figure 38: It is impossible to control actuators at the edge of the mirror using local control as the sections would fall outside the surface of the mirror.

outputs from a step response showed to be unstable independent of where on the mirror the section was positioned. In these test cases only one section had active control while all other actuators on the mirror were left uncontrolled.

4.5.1 Control development

The control was then expanded to handle many, overlapping, active local sections and the system robustness improved as more and more local sections were used. Finally, almost every actuator were center actuator for a 19 actuator local model. The relative forces for the individual sections were calculated and distributed, contributing to the forces generated from other center actuators in neighbour sections. When the overlapping sections were evenly spread over the whole mirror surface a stable process was reached. Only the two hexagonal rings around the mirror center and the two circles closest to the mirror edge were left uncontrolled. These were left out since the local model of nineteen actuators would be mismatched on the surface of the mirror. The geometry of the sections makes it impossible to have an active section at the edge of the mirror surface, see Figure 38. The same

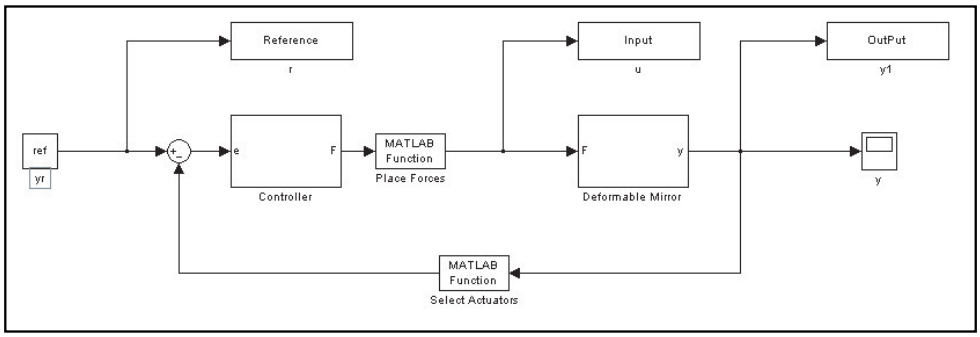

Figure 39: Simulink model for the full mirror control simulations.

problem occurs for the center of the mirror as the origin is fixed and can not be controlled. Problems with control of the edge and the center of the mirror calls for a new, smaller, local model. Leaving these actuators uncontrolled is not an option as tests showed that the edges starts to wrench because of the poor damping in the CFRP material.

The hexagonal ring next to the edge and the second hexagonal ring from the center are controlled using a smaller version of the local model[19]. This model contains only seven actuators using one active center actuator and its closest hexagonal (six actuator) ring. A local symmetrical model for the edge of the mirror is however impossible to produce and these actuators are thereby controlled using SISO control alone. The circle closest to the center of the mirror were left uncontrolled. This is physically possible since the center is fixed and the waves are damped as they are reflected on the supported section. This leaves the full control of the mirror with two different types of local model control and one type of SISO control in the outer hexagonal ring.

4.5.2 Implementation of the full mirror control

The multivariable mirror system has been implemented in Matlab[20] and Simulink, using its well-known qualities for matrix manipulations. Model and control of the mirror have then been tested, verified and improved using the output data from Simulink. A screen shot of the simulation block is at

[19]This model was made in the same fashion as the local 19 actuator model.

[20]Sources used for Matlab programming was, besides of the Matlab help function, [14] and [12].

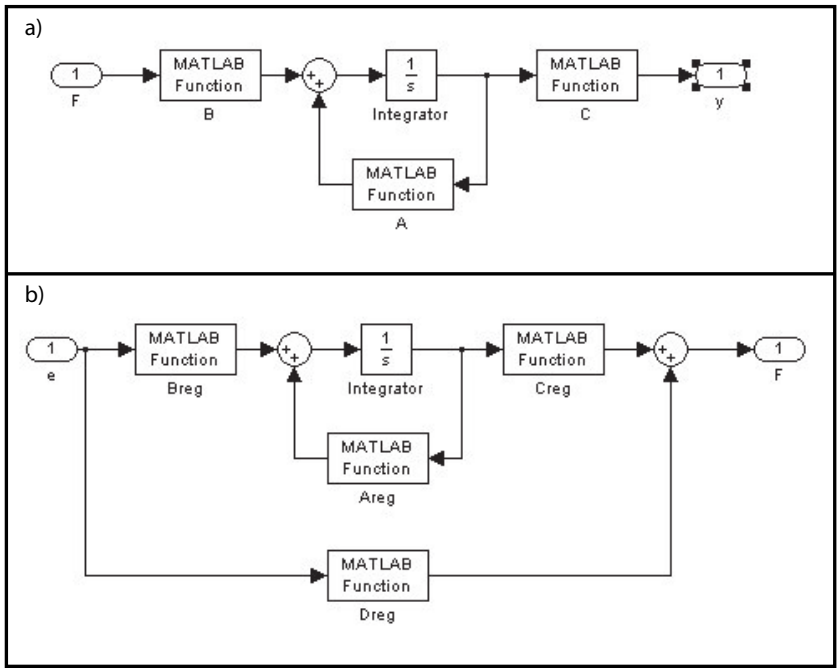

Figure 40: a) The full mirror model realization. b) The model of the controller.

display in Figure 39. The block yr contains a command signal to the mirror. The reference signals could for example form a coneshaped step response (see Figure 42) or contain variable amplitudes for every actuator very much like a real reference coming from adaptive optics reconstruction[21]. The references, yr are subtracted with the deformations, y, giving the control errors, e, for every actuator position. The error enters the control block generating forces, F, for each and every central actuator. As the SISO control was found inadequate, these forces are used to form force distributions over all mirror sections. There are now 19 force signals for every section coming out of the controller. These, however, are not sorted nor added to form the total input of 3162 forces. The sorting and addition of section forces are handled in the *Place Forces* block. The sorted inputs are then fed into the mirror model to influence it (see figure 39), giving the deformation output vector. The *Select Actuators* block makes sure that only the deformations controlled are fed back.

The controller block and the deformable mirror block are subsystems containing the necessary matrix manipulations. The realizations of the models

[21]Such a test would use a different Simulink approach.

are shown in Figure 40. The A-, B- and C-matrices in the mirror model are the modal model matrices (see Section 3). But how are the control matrices A_{reg}, B_{reg}, C_{reg} and D_{reg} designed?

The full mirror controller contains three different compensation links. The first for the control of the standard local model, the second for the smaller local model and the last for the SISO compensations on the edges. The filters have all been chosen to give the small systems as good phase margins as possible. Once the compensation links have been designed they are transformed into state-space representation in Matlab. Every controller is then represented by A_r-, B_r-, C_r- and D_r-matrices. In order to construct comprehensive control matrices for the full model, these are placed into corresponding matrices. The new matrices are built with the representations of the respective compensation links on the diagonal. Take for example the compound control matrix A_{reg}, which is built as below in Equation 26. Here A_{r1} represents the controllers of the standard local models. A_{r2} belongs to the small local model controllers and A_{r3} symbolizes the SISO controllers for the actuators on the edge.

$$A_{reg} = \begin{bmatrix} A_{r1} & 0 & \dots & 0 & 0 \\ 0 & A_{r1} & \dots & 0 & 0 \\ \vdots & \vdots & \ddots & \vdots & \vdots \\ 0 & 0 & \dots & A_{r2} & 0 \\ 0 & 0 & \dots & 0 & A_{r3} \end{bmatrix} \tag{26}$$

The other control matrices are assembled using the same method. A full representation of the controller matrices can be found in Appendix A.7 and the control design code in Appendix A.6.

4.5.3 Results of the full mirror control

In order to analyse the control of the full mirror model, several step response tests were performed (see the output from a typical step response in Figure 41). The command signal was formed as the shape of a cone on one section (see Figure 42). The center actuator for the section is given a reference of 12 nm and the first hexagonal ring around this actuator containing six actuators is given a corresponding signal of 10 nm. Then the third hexagonal ring with 12 actuators are obliged to a command signal of 5 nm. The cone shape was used taking the mirror's ability to bend into consideration. Hence, the

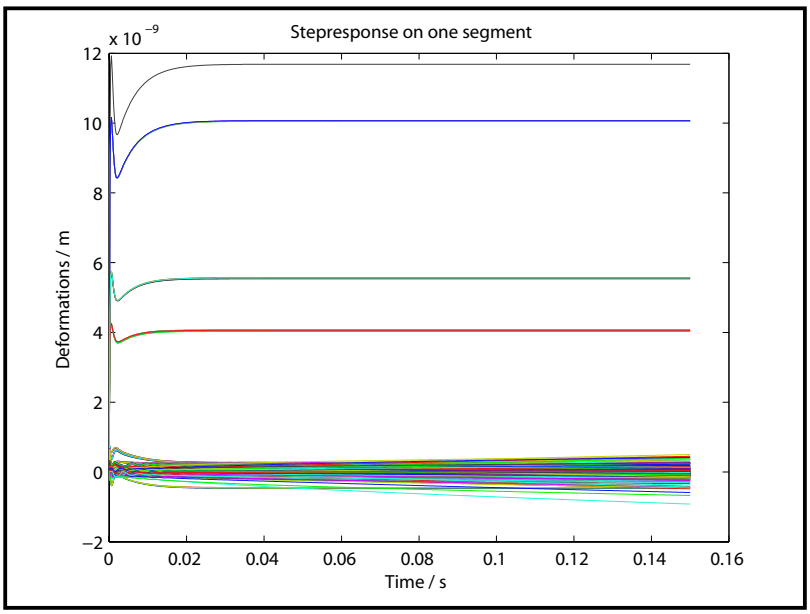

Figure 41: The output of a step response test using the local control on the full mirror model. The highest curve corresponds to the center actuator of a 19 actuator section. The next one refers to the second hexagonal ring and the two transients around 5 nm refer to the third ring. See the command signal in Figure 42.

mirror is not forced to be bent in a way that the structure can not tolerate with too much divergence of deformations between adjacent actuators. Even though these precautions were taken, quite a few strange behaviours could be viewed, see Figure 41. Consider the output behaviour of the actuators commanded to 5 nm. Their step responses are divided into two groups. None of these are ending at the correct value. The phenomena disappeared as the control was examined on the larger Guyan reduced mirror model. It was this feature and some other strange results[22] that led to a model substitution. As the 2002 modes model did not prove to be absolutely accurate earlier in Section 3.2 no time was spent examining the strange behaviors further[23].

There were also problems with some actuators given zero reference signal. They seemed to wander off and grow, but it is hard to tell what happens and which actuators the growing deformations correspond to. Are the main

[22]For example the stationary error of the center actuator.

[23]When seen in the light of these facts, one might argue that the cone shaped reference was probably unnecessary. This, however, was not examined further in this thesis and the cone was used in all step response tests.

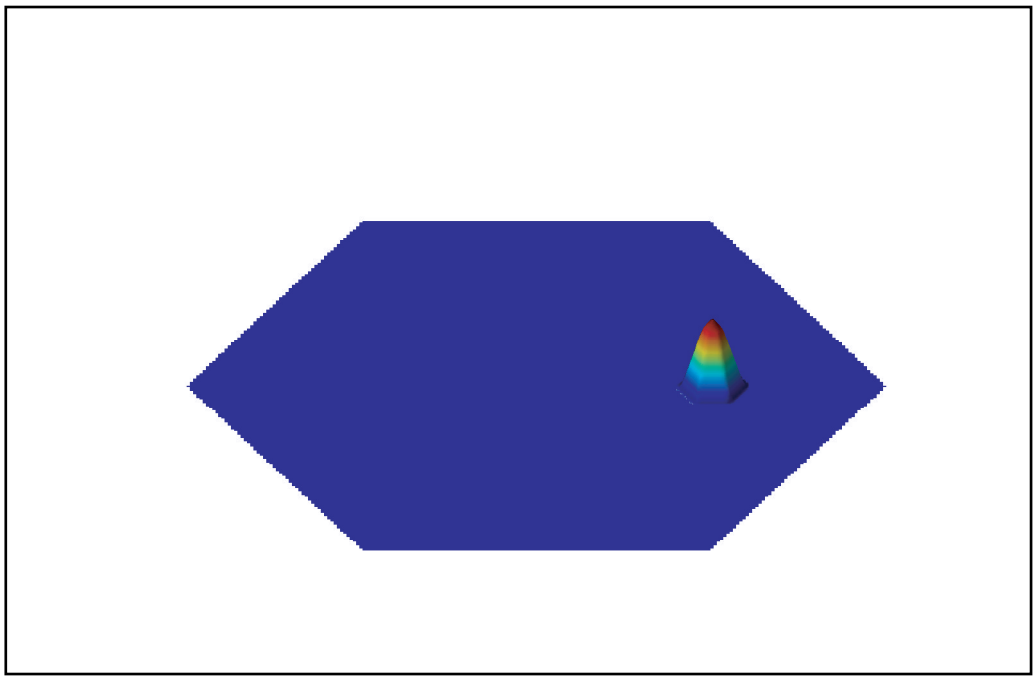

Figure 42: The command signal used throughout this thesis in step response tests on the full mirror. Note that the deformation dimensions are exaggerated in comparison to the mirror size.

problems caused by poor edge control or is it perhaps the uncontrolled actuator ring in the center of the mirror that proves to be inadequate? One can of course draw more conclusions by a further examination of individual step response outputs, but the whole picture may be hard to grasp then. In order to simplify the analysis of the mirror dynamics, a motion picture in three dimensions was made. The outputs and time were stored in a specific matrix. Using the information on where the actuators are placed and the Matlab command *trisurf*, one can draw new pictures of the mirror deformations for every time sample. A movie is then created looping the images. This approach proved to be of great use in this thesis since it was possible to see exactly how systems like the one in Figure 41 behaved. The full Matlab script can be viewed in Appendix A.5. The movie showed very clearly that the mirror edges and center had divergent outputs. The mirror behaviour looked very strange in the movie with growing waves in the outermost and innermost actuator rings. These behaviours disappeared in large after the model change.

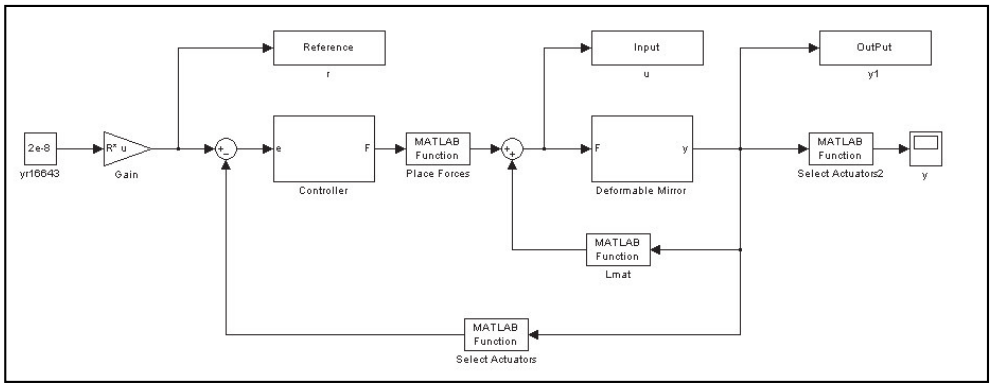

Figure 43: Simulation of the full mirror control using state feedback in Simulink.

Another curious mirror behaviour is transient dips in the step response plot (see Figure 41). This quality was preserved even when the model was substituted. One possible reason is that the closed loop have zeros which have a large influence on the transients. It seems desirable to avoid this unwanted feature which might make the control less accurate.

4.6 Control using state feedback

A variant of state feedback control was tested in order to further improve the system robustness. The idea was to use the velocities of the mirror deformations. It is known that damping can be modeled as $-d\dot{x}$, where d is the damping coefficient and $\dot{x}$ is the velocity of a variable, e.g. the deformation as in this case. This characteristic may be used in the mirror control in a state feedback fashion. The combined compensation/distribution control of the mirror will thereby be further combined with this state feedback control as a damping contribution to the control signal. The damping coefficients have been selected by looking at the characteristics of a local model. A force in the center actuator generates radial waves. It would therefore be advisable to choose the same damping coefficients for every actuator position in the hexagonal ring closest to the active actuator. The same thing would hold for the ring just outside that one. As all sections are considered, each actuator will have damping contributions from several rings resulting in a final damping coefficient. As mentioned before, the edge and the center of the mirror lack active sections. Consequently, the actuators positioned in the middle of the mirror have larger feedbacks through the L matrix than actuators at the edge and the center. All damping coefficients d_i are placed in the diagonal of a diagonal matrix L.

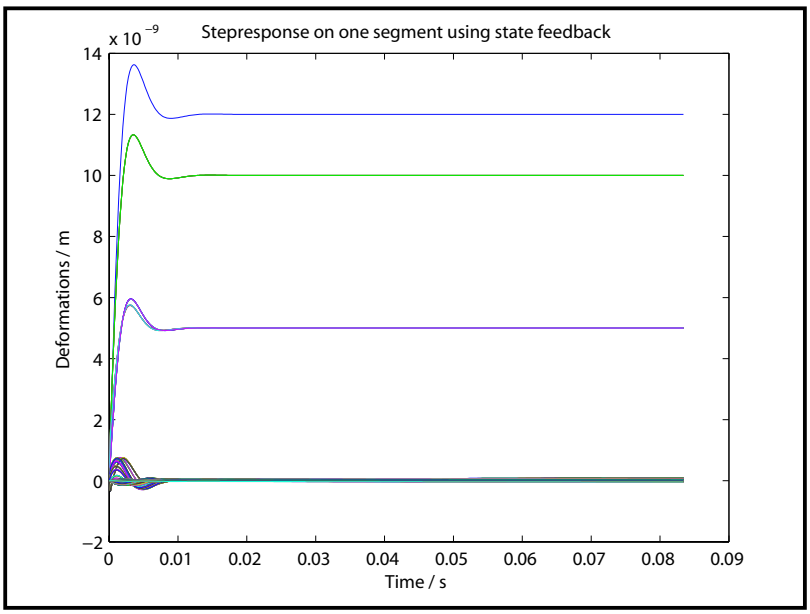

Figure 44: Deformation outputs of a step response test where a combined force distribution and state feedback control is used. The command signals are the same as in Figure 41 and can be viewed in Figure 42.

$$L = \begin{bmatrix} d_1 & 0 & \dots & 0 & 0 \\ 0 & d_2 & \dots & 0 & 0 \\ \vdots & \vdots & \ddots & \vdots & \vdots \\ 0 & 0 & \dots & d_{n-1} & 0 \\ 0 & 0 & \dots & 0 & d_n \end{bmatrix} \tag{27}$$

Multiplying this matrix with the deformation velocities gives the desired contribution to the control signal, i.e. $u_{extra} = -L\dot{x}$. It should also be mentioned that the velocities $\dot{x}$ could be used transforming the C-matrix (see Equation 14) into

$$C = \begin{bmatrix} \Phi & 0 \\ 0 & \Phi \end{bmatrix} \tag{28}$$

The Simulink view of the full system can be seen in Figure 43 were the velocities from every actuator are fed back through the L-matrix.

Comparing Figure 41 to Figure 44 of a step response using state feedback

leaves it obvious that the results are more attractive after the modification. The system with state feedback is slower in the initial stage but it approaches the static value in less time than the system with the force distribution alone. The error is also generally smaller in the state feedback case. The conclusion must be that the state feedback controller also made the total system more robust but that it need to be faster. The questions are whether or not a faster system can have the same robustness qualities and then how to achieve them?

4.7 Control using modal damping

The state feedback control strategy has qualities necessary to achieve good control for the complicated process that the deformable mirror represents. The L-matrix however, seems hard to tune so that the system bandwidth remains high. A guess is that the state feedback control damps all mirror modes and the question is if it is possible to take care of the most significant modes alone. The most significant modes of the local model can be identified by watching the modal states of the local model during a step response. Figure 45 shows a plot of the local model states. This gives a measure of how much each mode is triggered when the compensation link (for the center actuator) and the force distribution are used. The model has a total of 19 modes and the most significant of these are modes number 1, 3, 6 and 12. These can be viewed in Figure 46. With mode number 6 as the only exception, they are all rotationally symmetric. These are the only local modes that have this attribute. Thus, the significance of these modes is probably emanating from this special feature. This seems to be a reasonable guess since the actuators generate circular waves over the surface. The significance of the sixth mode on the other hand, remains a mystery. An iterative tuning of the control, however, demonstrated improved dynamics when this mode was damped.

Figure 47 shows that there is an obvious gain in taking care of the most significant modes. The convergence times are about the same, but the oscillations are now better damped and the amplitudes are significantly smaller. The approach used in this thesis was to damp the modal velocities multiplying them with negative damping coefficients. Actually, this is the same thing as the state feedback, the only difference is that the damping coefficients are chosen more carefully. The main benefit of this new approach would be that the control is more efficient.

It should also be mentioned that the modal control alters the force distribu-

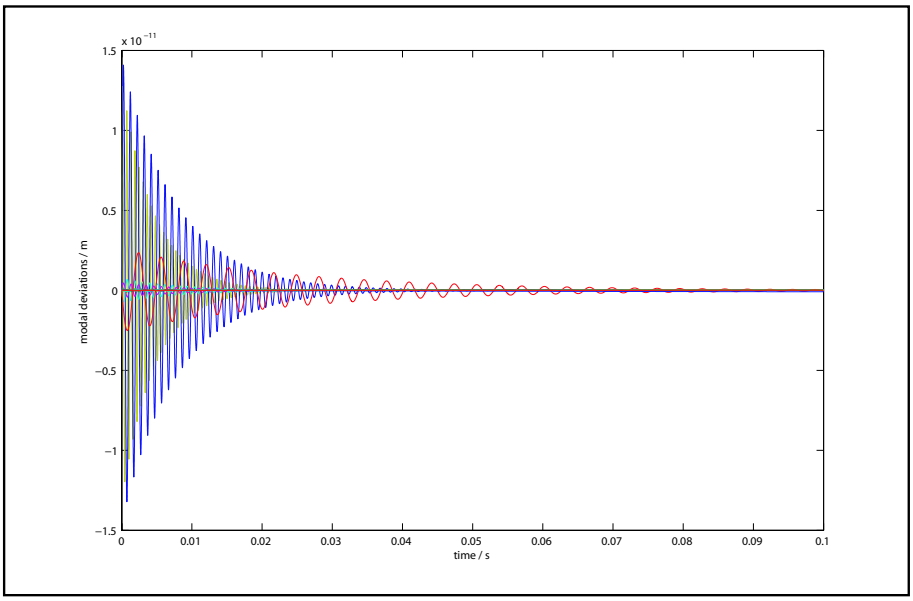

Figure 45: A plot of the modal states of the local model when the force distribution/compensation alone is being used during a step response.

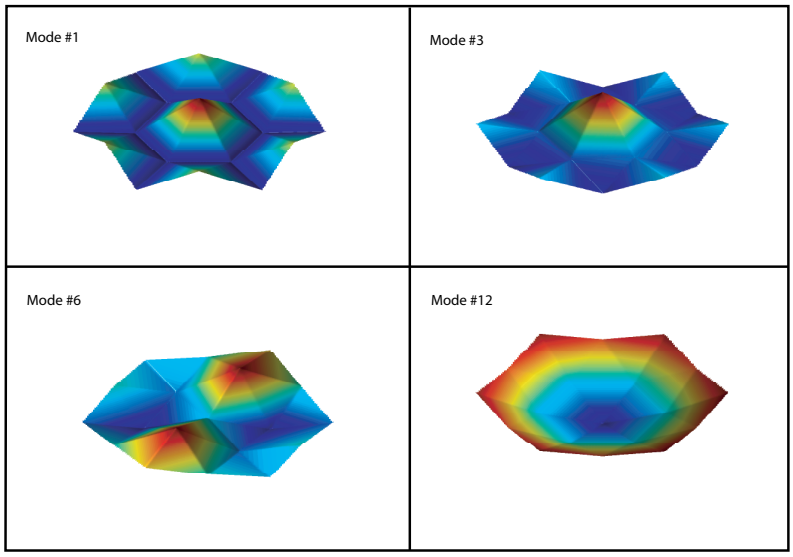

Figure 46: The four most significant local modes.

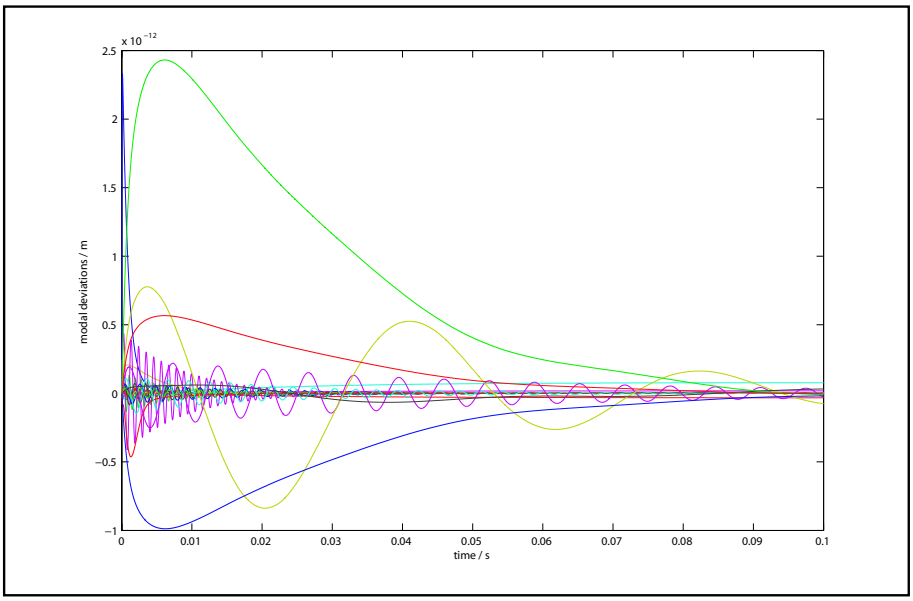

Figure 47: A plot of the same test as in Figure 45, but with modal damping.

tion needed to provide a static balance for the local model. This however, is not a problem since all sections have active control in the full mirror control.

It proved difficult to implement the modal controller on the full mirror model and there was not enough time in this thesis project to set up a functional controller of this type. Tests on the local model, however, have shown satisfying results and the modal damping strategy is therefore considered important to be investigated further in the future.

4.8 Control evolution results

During the course of control development many system transfer functions were studied. To get a good intuitive feeling of the benefits for different control strategies, this seemed to be a good initiative. In Simulink it is possible to get linearized transfer functions with e.g. input at the command signal and output at the process output using the control design tool. This was done for the local systems using the different control strategies showing behaviours and contributions of the same[24], see Figure 48. The untampered system, without control and no feedback (yellow with many peaks), has bad

[24]Note that it was the open systems that were watched and that the transfer functions were from center actuator force to center actuator deformation.

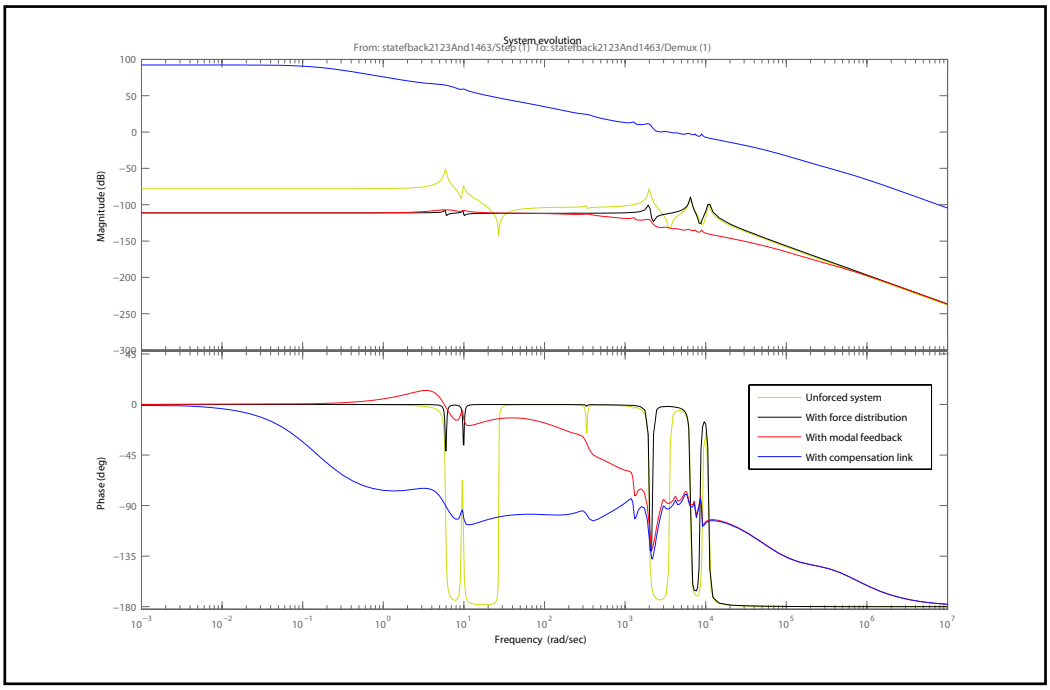

Figure 48: Bode diagram of systems resulting from the control evolution.

phase and includes several peaks and dips effecting the control with poor robustness as a result. When the force distribution was put on the mirror a more harmonic Bode plot presented itself (see the black system, with 3 distinct peaks, in the same Figure). Many of the magnitude peaks and dips at low frequencies have vanished and a better phase was received for higher frequencies leading to a more straightforward control. Modal feedback added further to these characteristics (the smooth red curve) with better damped resonance peaks as a result. The system was now almost behaving as a low pass filter without any resonances. This is a quite common appearance for many systems and also highly desirable. A new compensation link could then be designed to manipulate the system, receiving both increased low frequency magnitude and a feasible bandwidth. The system for a section being controlled using all strategies is represented by the blue system in the Bode diagram (the one with higher gain).

As the magnitude slope for the compensated system does not cross 0 dB more than once, a realization with a well determined bandwidth was achieved. Reading the Bode diagram one could then determine the bandwidth to 550 Hz and the phase margin to 87 degrees. With Section 4.1.1 in mind one

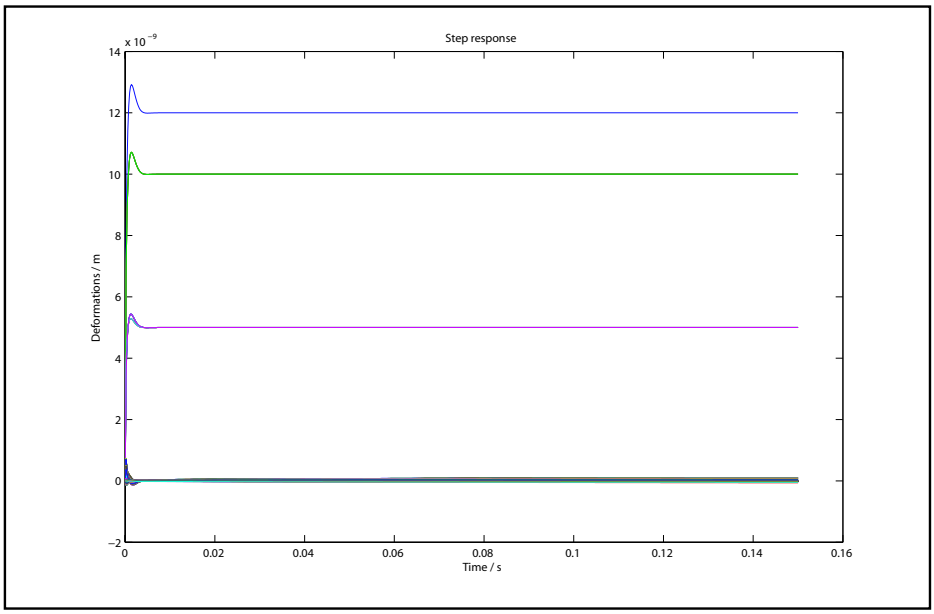

Figure 49: Step response using state feedback control with higher bandwidth. The same command signals as before are used.

can argue that the phase margin is too high. One should however consider that coupling effects might lead to worse phase margin than achieved in this analysis. A high phase margin may therefore be crucial and 87 degrees is perhaps not so bad. It should also be mentioned that the coupling effects are very much neglected throughout this thesis. The control of the full mirror however seem to verify that the SISO diagrams (from center actuator force to center actuator deformation) are the most important when analysing the systems. These are after all the ones controlled actively. The cross-coupling, however, deserves more attention and should therefore be considered in more detail in future research plans.

An important difference between the modal control approach and the others are that the compensation filter was chosen after both force distribution and modal dampings had been set. A compensation link could thus be tuned to fulfill the requirements of both faster control and reasonable phase margin leading to a better system overall.

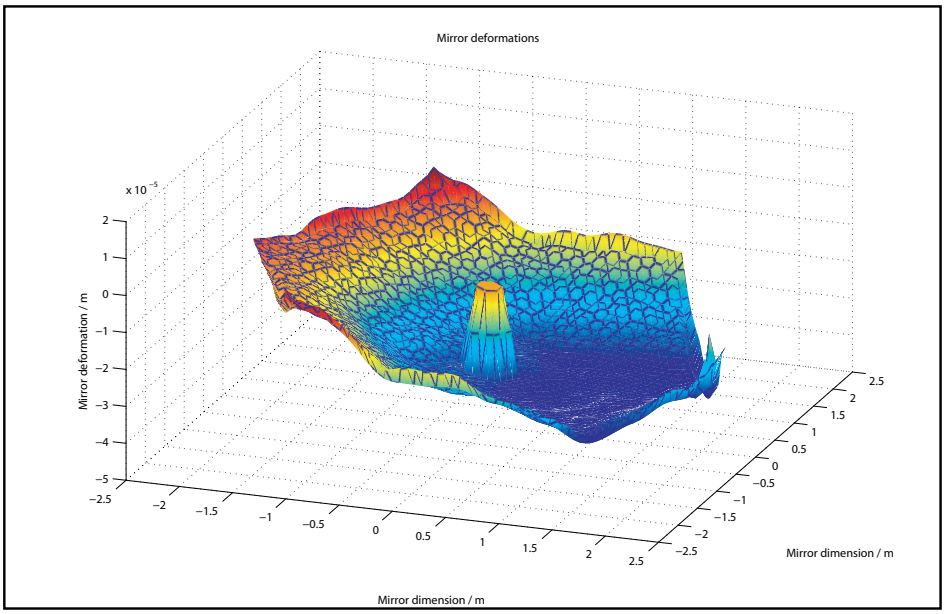

Figure 50: Realistic deformable mirror command signals was tracked.

4.9 State feedback control with higher bandwidth

As the implementation difficulties of the modal control approach led to a dead end, an old idea was reconsidered. The state feedback solution in Section 4.6 proved to be too slow. The control evolution in the previous section, however, showed that the compensation link could simply be modified to receive a faster system. Since the state feedback controller is very similar to the modal controller it seems reasonable to believe that at least some modal damping will result from that control as well. The state feedback control was therefore once again considered after an increase in the compensation filter gain.

Step response tests on the full mirror (see Figure 49) showed that an approximate bandwidth of 800 Hz could be achieved and that the robustness was intact, if not better. The estimated bandwidth was determined using Equation (30), in the next section. A feasible mirror control, with a fast, robust system, is hereby achieved. In order to examine if the specifications were met, the controller was to be tested for realistic telescope reference signals

The final RMS-value was determined taking the RMS for every actuator po-

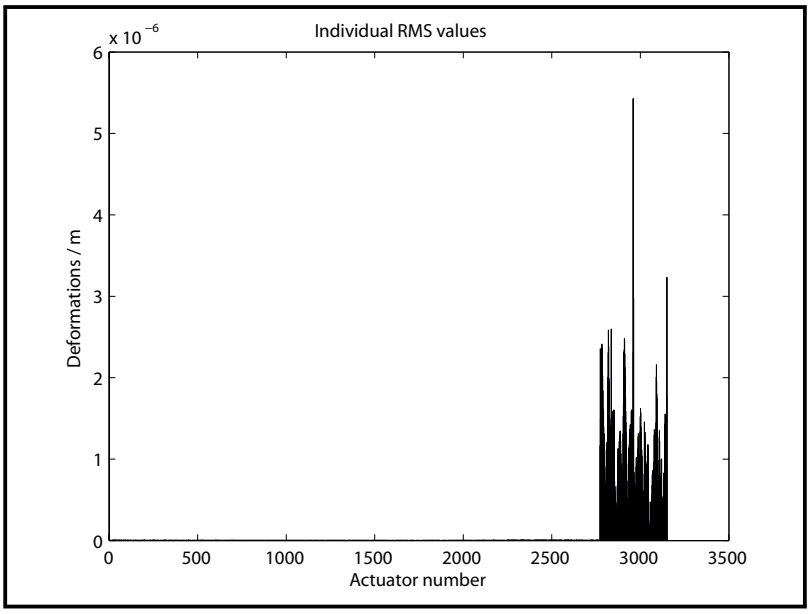

Figure 51: Individual RMS values for the actuators. The higher number the actuator has, the closer to the edge it is situated.

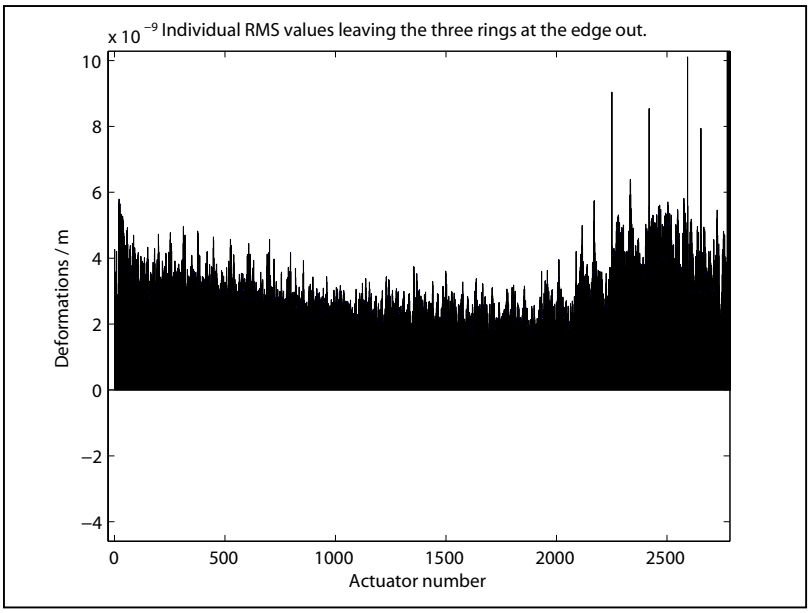

Figure 52: Individual RMS values for the actuators. Three rings at the edge were left out in this zoom in of Figure 51.

sition and then the RMS over all these values. It was then determined to 395 nm which is not that flattering since the specifications require a RMS value of at most 80 nm for IR light. Further examinations of the individual RMS values (see Figure 51), however, showed that there were still some problems controlling the edge. The errors for the actuators located in the three outermost hexagonal rings have RMS values of at most 5.5 μm. This has a great impact on the final RMS value. When Figure 51 was zoomed in, leaving these three rings out, a far better result was observed, see Figure 52. The RMS values were less than 10 nm for each of these actuators and the total RMS was just 3.2 nm, indicating that the specifications were met for these actuator positions.

The problems with the edges, however, still remains and at this point no true explanation exists although there are several possible reasons. The references at the edge may not have been generated to match the mirror surface to an acceptable degree. Furthermore, the smaller local model for the edges should once again be studied and verified. This model might not describe the dynamics of the mirror edge as expected. The SISO control of the edge actuators may also cause trouble and asymmetric local models are perhaps advisable to use in order to create better edge control.

Due to lack of time in the end of this thesis project, the realistic references were only tracked for 0.2 s[25]. The full time series, however, lasts for more than 8 seconds. This experiment might therefore not be representative for the true RMS value. A full scale experiment should therefore be launched to see whether or not the control is feasible.

4.10 Control difficulties

4.10.1 Fast control and model reliability

Due to an unfortunate programming flaw the SISO control for the edge was set to a bandwidth of several thousand Hz. The behaviour was detected as the edge control showed to be better than ever expected. This raised the question whether or not the overall mirror controller was too fast as well. The compensation filters for the mirror controllers was therefore used as SISO controllers. It showed that these compensation filters gave a stable SISO system with fantastic properties. Taking an approximate bandwidth of the system however, showed that it was set in a frequency span where the model is not reliable (see Figure 53). The approximate bandwidth was

[25]Simulation time approximately four days at a Pentium 2.4 GHz with 1024 Mb memory.

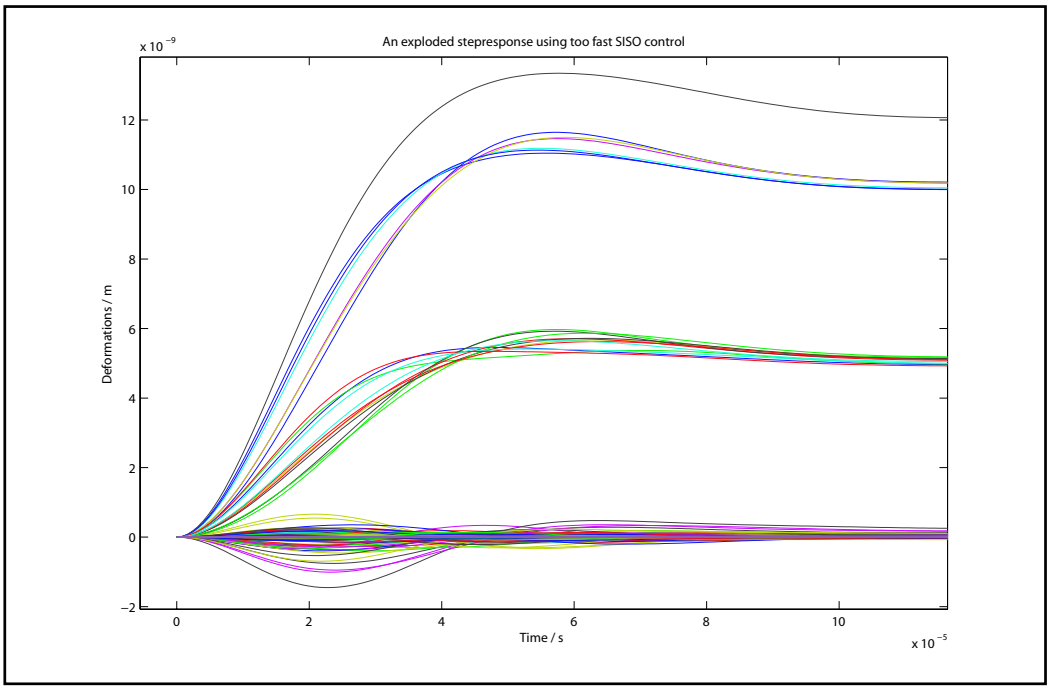

Figure 53: A magnified step response showing that the SISO control on the full mirror is too fast to be adequate.

defined as

$$\omega_b = \frac{1}{\tau} \tag{29}$$

where τ is the time constant of the system. The mirror process is thereby approximated as a first order system. A calculation of the SISO system bandwidth (in Hz) gives

$$f_b = \frac{1}{0.63 \cdot 2.2 \cdot 10^{-5} \cdot 2 \cdot \pi} \approx 7200 \ Hz \tag{30}$$

which is too high. The 2002 model should not be used over 1500 Hz and the same thing counts for the Guyan reduced model. This new SISO approach could thereby be disregarded as before. It was also proved that lower filter bandwidths gave an unstable system once again.

The worry was whether or not the rest of the control systems developed were defined for the models. Step response tests, however, showed that the approximate bandwidths were within a reasonable model frequency span. This would also prove that the section control approach is useful.

4.10.2 Cumbersome simulations

The Simulink simulations were realized using the Matlab solver *ode*4 with a fixed step time of $4 \cdot 10^{-6}$. The final control system had several thousand controllers of order three or less. The Guyan reduced system has an order of more than 6000 and the L-matrix containing all damping coefficients adds further to the complexity of the final system. All of these features adds to the total simulation time of the full mirror control. A simulation of 0.2 s took for instance more than two days to finish. Different simulations were therefore carried out at the same time at several computers in a local network .

5 Recommendations on future research

The research on deformable mirrors in Lund is still in its initial stage and more research has to be done before the final control objectives are reached. This thesis has given valuable clues as to what needs to be done in the future.

The main part of this thesis was the mirror control and the modeling studies were therefore not as extensive as will be needed in the future. The current models should be analysed in detail to find out whether or not they are representable for the real mirror and if a further model reduction might be a possible next step. A further, relevant, reduction of the full model order would be very welcome since it would simplify the analysis and control system design. Grocott's reduction [11] was based on the symmetrical properties of the MMT mirror. It may be possible to apply a similar reduction to the hexagonal Euro50 mirror. Wodek K. Gawronski's book, *Dynamics and Control of Structures* [10], is also recommended for further studies on e.g. model reduction. Further a model with time delays needs to be considered and the models should also be extended to include dynamics of the voice coil actuators as well as the capacitive gap sensors[26].

The analysis of the model needs to be extended to cover optimal sensor and actuator placement[27], examining controllability and observability Gramians along with system singular values. The cross coupling effects should also be considered in detail, especially when visual light adaptive optics is considered. The control system for visual light will also give a system with much more actuators.

Future development of the deformable mirror control should consider the use of more complex MIMO controllers, for instance LQG- or H_∞ control. The local models should provide the forum necessary to perform this. A complicated controller will, however, add more computer calculations. The simulations should then be made more efficient. It would also be necessary to include observers in order to determine deformation velocities. This will for instance be needed in order to use the state feedback on a real mirror.

The future deformable mirror research at Lund University will consider the control of a prototype mirror with 7 operating actuators. However, sooner or later there will also be a need to verify the control on a mirror with more

[26] Both when collocated with the actuators (as in this thesis) and located between.
[27] See for instance [10].

dynamic features. In order to reach the science level needed to control this mirror, a more long-term project should be started. Such studies should be run by a group of scientists and Ph.D./Master Thesis students[28]. The Ph.D. students could e.g. base their studies on the dynamics of flexible structures. A future cooperation with some commercial companies and/or other ELT project groups might also be advisable.

[28]Compare with the MMT group.

6 Main results and conclusions

Controlling the large deformable Euro50 mirror showed to be a formidable quest. The mirror has almost a thousand eigenmodes within the expected controller bandwidth and a modal model approach was extremely cumbersome considering computer calculations. Most of the problems however, could be overcome by the use of sparse matrices and Matlab functions supporting these.

Two large modal models were used in this thesis, the 2002 mode model and the Guyan reduced model. Model verification showed that the Guyan Reduced model had better static performance. It also showed more logical simulation results. The model should, however, not be used at too high frequencies since model errors are more significant there. In order to simplify the analysis of the MIMO control based on the full mirror model, a local mirror model was derived from the Guyan reduced model.

The control of the large deformable mirror needs a closed loop bandwidth of at least 500 Hz and an RMS-value of at most 80 nm. Four control approaches were used to find a solution. SISO control of actuator families gave an unstable system[29]. Force distributions, together with compensation filters, applied on mirror sections over the mirror gave a stable but not so accurate step response. In order to damp the system, a state feedback of deformation velocities was used as well and showed to be effective but slow. The last modal damping state feedback approach showed excellent behaviour on the local model but was never realized on the full model due to a complicated implementation. An idea sprung from this control led to further tests of the velocity feedback. The compensation links had higher bandwidth this time thus giving a fast enough step response. Results from tests with realistic command signals were then carried out and showed that the system could match the specifications for all actuator positions but for the mirror edges. The results give hope for the future research and the edge difficulties should not prove to be too hard a problem to solve.

[29]Very much like Grocott predicted [11]. See Section 1.5.3.

References

[1] MULTIPLE MIRROR TELESCOPE (MMT). URL: http://www.si.edu/archives/ihd/videocatalog/9542.htm (Accessed March 10, 2005).

[2] Adaptive Optics: Why?, 2002. URL: http://cfao.ucolick.org/ao/why.php (Accessed March 10, 2005).

[3] Euro 50, 2004. URL: http://www.astro.lu.se/~torben/euro50/ (Accessed March 10, 2005).

[4] Evolution of Telescopes, 2005. URL: http://www.infoplease.com/ce6/sci/A0861466.html (Accessed March 10, 2005).

[5] Torben Andersen and Holger Riewaldt. The Euro 50 Secondary Mirror, 2004. Lund Observatory, Lund University, Sweden.

[6] Torben Andersen et al. EURO 50 - A 50 m Adaptive Optics Telescope, 2003. ISBN 91-631-4317-8.

[7] G. Brusa et al. Adaptive secondary P30 prototype: laboratory results, 1998. Osservatorio Astrofisico di Arcetri et al., Firenze et al., Italy.

[8] G. Brusa et al. The adaptive secondary mirror for the 6.5m conversion of the Multiple Mirror Telescope, 2001. Osservatorio Astrofisico di Arcetri et al., Firenze et al., Italy.

[9] Roger A. Freedman and William J. Kaufmann III. Universe, 2002. Sixth edition, ISBN 0-7167-4647-6, W.H. Freeman and Company: New York.

[10] Wodek K. Gawronski. Dynamics and Control of Structures, A Modal Approach, 1998. ISBN 0-387-98527-1, Springer: New York.

[11] Simon C.O. Grocott. Dynamic Reconstruction and Multivariable Control for Force-Actuated, Thin Facesheet Adaptive Optics, 1997.

[12] Fredrik Gustafsson and Niclas Bergman. MATLAB - for Engineers Explained, 2002. ISBN 1-85233-697-8, Springer: London.

[13] Tore Hägglund. Reglerteknik AK, Föreläsningar, 2002. Department of Automatic Control, Lund University, Sweden.

[14] The MathWorks. MATLAB - The Language of Technical Computing, Using MATLAB Graphics, 2000. Version 6.

[15] Anders Rantzer. Lecture 3, 2003. Lecture Notes in the Computer-Controlled Systems Course. Department of Automatic Control, Lund University, Sweden.

[16] Olof Sandberg. Controlling the Secondary Mirror Cell of the Euro 50 Project using an Inertial Measurement Unit, 2005. Master's Thesis, Department of Automatic Control, Lund University, Sweden.

[17] John T. Spanos and Walter S. Tsuha. Selection of Component Modes for Flexible Multibody Simulation, 1991.

[18] Roger Svahn. Actuator Servos for Deformable Mirrors, 2005. Master's Thesis, Department of Industrial Electrical Engineering and Automation (IEA), Lund University, Sweden.

A Matlab programming files

A.1 State space modal model derivation

```
%#################################################################
%Creates the A-,B- and C-matrices for the 2002 mode model,
%using the FEM model.
%Authors: Fredrik Bjöörn & Olof Garpinger
%#################################################################
clear

%Load nodenumbers,
%x-, y- and z-coordinates together with deformations
%for the mirror in z for all 2002 modes
load M2-modal_a_modes;

%Load the eigenfrequences for all 2002 modes
load M2-frequencies.txt;
nbr_a = 3168; %Number of actuator nodes
nbrmod = 2002; %Number of modes taken into account

%The natural frequency vector in rad/s
omega = [2*pi*M2_frequencies(:,2)];

%The normalized modal matrix
Phi = [a_modes(:,5:nbrmod+4)];

%-----------------------------------------------------------------
%The A-Matrix
%-----------------------------------------------------------------
%The approximate damping factor for the Carbon Fiber Reinforced
%Polymer mirror
Z = 0.02;
%A = [0 I; -(omega)^2 -2*Z*omega]
A = [zeros(nbrmod) eye(nbrmod);...
    diag(-omega.*omega) diag(-2*Z*omega)];

%-----------------------------------------------------------------
%The B-Matrix
%-----------------------------------------------------------------
%B = [o; Bm]; Bm = inv(Mm)*Phi'*B0 = Phi'*B0, since Mm = B0 = I
```

```
B = [zeros(nbrmod, nbr_a); Phi'];
save ABmat A B %Save the A- and B-matrices temporary

%Allocate memory
clear a_modes e_modes s_modes omega M2_frequencies A B

%-----------------------------------------------------------------
%The C-Matrix
%-----------------------------------------------------------------
%y = Coq*q + Cov*qdot, Cov = 0 => the deformations are measured
C = [Phi zeros(nbr_a, nbrmod)]; %C = [Phi 0]
save Cmat C
clear

load ABmat
load Cmat

%Save the A- B- and C-matrices in a file
save ABCmatrices_2002a A B C

delete ABmat.mat %Deletes temporary files from disk
delete Cmat.mat
```

A.2 Verification of the mirror model

```
%#################################################################
%The static gain is used for comparison between the State Space
%Model and the more complex FEM model. Two different test
%cases are used to measure the residuals between the two models
%The residuals are plotted in Figures.
%Authors: Fredrik Bjöörn & Olof Garpinger
%#################################################################
clear
load ABCmatrices_2002a
load Dmatrix

%G(s) = C*(sI-A)^(-1)*B,
G0 = -C*(A\B); %The static gain, G(0) = -CA^(-1)B

save staticgain_2002a G0 %Save the gain to file

%-----------------------------------------------------------------
%Determines the static deformations for the State Space Model
%of the secondary mirror using the first test case force vector
%-----------------------------------------------------------------
clear

%Creates a force vector for the verification
load M2-modal_a_modes; %Load the actuator modes
nbr_a=3168;
F = zeros(nbr_a,1); %Create the force vector

%Find the numbers of the right force actuators and give them
%predetermined test forces
F(find(a_modes(:,1)==6203),1)=-10;
F(find(a_modes(:,1)==6653),1)=-10;
F(find(a_modes(:,1)==7113),1)=-10;

clear a_modes nbr_a %Allocate memory

%Load static gain of the mirror model
load staticgain_2002a

%Find the static deformations, i.e. y(inf)=G(0)*F
```

```
delta1 =  G0*F;

%Save the deformations
save deformations1_2002a delta1

%-------------------------------------------------------------
%Determines the static deformations for the State Space Model
%of the secondary mirror using the second test case forcevector
%-------------------------------------------------------------
clear

%Creates a force vector for the verification
load M2-modal_a_modes; %Load the actuator modes
nbr_a=3168;
F = zeros(nbr_a,1); %Create the force vector

%Find the numbers of the right force actuators and give them
%predetermined test forces
F(find(a_modes(:,1)==12783),1)=-1;
F(find(a_modes(:,1)==14715),1)=-1;
F(find(a_modes(:,1)==16863),1)=-1;
F(find(a_modes(:,1)==14739),1)=3;

clear a_modes nbr_a %Allocate memory

%Load static gain of the mirror model
load staticgain_2002a

%Find the static deformations, i.e. y(inf)=G(0)*F
delta2 =  G0*F;

%Save the deformations
save deformations2_2002a delta2

%-------------------------------------------------------------
%Comparisons are made between the more advanced FEM model and
%the State Space Model in various plots
%-------------------------------------------------------------
clear

%Load M2 deformations from both the FEM model and the State
```

```
%Space model for both test cases
load deformation_H1_2002a %FEM deformations case 1
load deformation_H2_2002a %FEM deformations case 2
load deformations1_2002a %State Space deformations case 1
load deformations2_2002a %State Space deformations case 2

%Plot mirror deformations
load M2-modal_a_modes.mat %Load actuator modes

x = a_modes(:,2); %Get x-coordinates
y = a_modes(:,3); %Get y-coordinates
tri = delaunay(x,y); %Delaunay triangulation

%Triangular surface plot of the differences between the first
%deformations
trisurf(tri,x,y,dz1-delta1,'EdgeColor','none')
title('The differences between the first deformations')
zlabel('Deformation differences in meters')

figure

%Triangular surface plot of the differances between the second
%deformations
trisurf(tri,x,y,dz2-delta2,'EdgeColor','none')
title('The differences between the second deformations')
zlabel('Deformation differences in meters')

maxcase1=max(dz1-delta1) %Maximum deformation, case 1
maxcase2=max(dz2-delta2) %Maximum deformation, case 2
mincase1=min(dz1-delta1) %Minimum deformation, case 1
mincase2=min(dz2-delta2) %Minimum deformation, case 2

meancase1=sum(abs(dz1-delta1))/length(dz1) %Mean, case 1
meancase2=sum(abs(dz2-delta2))/length(dz2) %Mean, case 2

%Contour plots of the deviations between the two models
xlin = linspace(-2.2,2.2,150);
ylin = linspace(-2.2,2.2,150);
[xm ym] = meshgrid(xlin,ylin);

%Interpolation function, puts data on grid
```

```
zm1 = griddata(x,y,dz1-delta1,xm,ym);
zm2 = griddata(x,y,dz2-delta2,xm,ym);

figure
[cs1,h1]=contour(xm,ym,zm1);
figure
[cs2,h2]=contour(xm,ym,zm2);
```

A.3 Transfer functions for the actuators located from the center to the edge of the deformable mirror

```
%#################################################################
%Find the actuator numbers from x=0 to x= 2.2 when y=0
%Authors: Fredrik Bjöörn & Olof Garpinger
%#################################################################

vec(1)=1; %The first actuator number=1
xvec(1)=vec(1);
%There exists 32 actuators from the middle of the mirror to
%the edge
for k=1:31

    %Returns all neighbours to the actuator
    vec = neighbournodes(vec(1));

    %Puts the actuator number of the neighbour to the right
    %(vec(1)) into a vector, xvec
    xvec(k+1) = findnodeplace(vec(1));
end

%-----------------------------------------------------------------
%Save the Bodeplots for the transfer functions from actuator
%force to deformation using the actuators above.
%-----------------------------------------------------------------

load ABCmatrices_2002a A
freqv = logspace(-1,4,500); %Frequencies in rad/s
sI = i*sparse(eye(length(A))); %i*I
A = sparse(A);

for l=1:length(xvec) %Use the l:th actuator
    load ABCmatrices_2002a B C
    B = sparse(B(:,xvec(l))); %Using the xvec(l):th column
    C = sparse(C(xvec(l),:)); %Using the xvec(l):th row

    for j=1:length(freqv)
        temp = freqv(j)*sI-A; %i*w*I-A
        %Calculate the transfer function for a frequency w
        G(j) = C*(temp\B);
```

```
        pause(0.2) %Allow Ctrl-c
    end
    Gs(:,1)=full(transpose(G)); %From sparse to full matrix
end
save Gsmatrix Gs
```

A.4 SISO compensation filters for the actuators

```
%#################################################################
%Compensation link for the first actuator - Family 1
%Authors: Fredrik Bjöörn & Olof Garpinger
%#################################################################
load Gsmatrix %Transfer functions are loaded

%The transfer function containing the first actuator is
%sorted out
G=Gs(:,1);

%Frequency vector containing 700 points between 10^-1 and 10^4
freqv = logspace(-1,4,700);

%Creation of or conversion to Frequency Response Data model
Gsys = frd(G,freqv);

K=5e4; %Static gain
w1=7; %Locations for the inverted Notch filter
z=0.25; %Damping for the inverted Notch filter
s=tf('s'); %Specifies the transfer function H(s) = s

%Transfer function for the inverted Notch filter
Gk1 = K*(s+w1)^2/(s^2+2*z*w1*s+w1^2);

%Compensation links
Bandpas=(Gk1^1);
Phasedec=(s+2)/(s*(s+400));

sys = K*Bandpas*Phasedec*Gsys; %The compensated system
%The controller
[numreg1,denreg1] = tfdata(K*Bandpas*Phasedec,'v');

%Plotting the Bode plot of the system and the controller
margin(sys)
hold on

bode(Bandpas*Phasedec,'r')
grid on
hold off
```

```
%#################################################################
%Compensation link for the second to the fourth actuator
%Family 2
%#################################################################

K=8.9; %Static gain
w1=7; %Locations for the inverted Notch filter
w2=15;
w3=50;
w4=150;
z=0.25; %Damping for the inverted Notch filters
s=tf('s'); %Specifies the transfer function H(s) = s

%Transfer functions for the inverted Notch filters
Gk1 = K*(s+w1)^2/((s)^2+2*z*w1*s+w1^2);
Gk2 = K*(s+w2)^2/((s)^2+2*z*w2*s+w2^2);
Gk3 = K*(s+w3)^2/((s)^2+2*z*w3*s+w3^2);
Gk4 = K*(s+w4)^2/((s)^2+2*z*w4*s+w4^2);

%Compensation links
Bandpas=(Gk1^2*Gk2^1*Gk3^1*Gk4^1);
Phasead = ((s+4))/((s+80));
Phasedec=(s+4)^2/((s+0.01)^2);

%#################################################################
%Compensation links for the fifth to the eleventh actuator
%Family 3
%#################################################################

K=2.2; %Static gain
w1=10; %Locations for the inverted Notch filter
w2=18;
w3=50;
w4=100;
w5=160;
z=0.45; %Damping for the inverted Notch filters
s=tf('s'); %Specifies the transfer function H(s) = s

%Transfer functions for the inverted Notch filters
Gk1 = K*(s+w1)^2/((s)^2+2*z*w1*s+w1^2);
```

```
Gk2 = K*(s+w2)^2/((s)^2+2*z*w2*s+w2^2);
Gk3 = K*(s+w3)^2/((s)^2+2*z*w3*s+w3^2);
Gk4 = K*(s+w4)^2/((s)^2+2*z*w4*s+w4^2);
Gk5 = K*(s+w5)^2/((s)^2+2*z*w5*s+w5^2);

%Compensation links
Bandpas=(Gk1^3*Gk2^3*Gk3^3*Gk4^3*Gk5^3);
Phasead = ((s+60))/((s+300));
Phasedec=((s+3)*(s+2))/((s)*(s+0.02));

%#################################################################
%Compensation links for the 12'th to the 22'nd actuator
%Family 4
%#################################################################

K=4.2; %Static gain
w1=30; %Locations for the inverted Notch filters
w2=50;
w3=100;
w4=150;
z=0.45; %Damping for the inverted Notch filters
s=tf('s'); %Specifies the transfer function H(s) = s

%Transfer functions for the inverted Notch filters
Gk1 = K*(s+w1)^2/((s)^2+2*z*w1*s+w1^2);
Gk2 = K*(s+w2)^2/((s)^2+2*z*w2*s+w2^2);
Gk3 = K*(s+w3)^2/((s)^2+2*z*w3*s+w3^2);
Gk4 = K*(s+w4)^2/((s)^2+2*z*w4*s+w4^2);

%Compensation links
Bandpas=(Gk1^2*Gk2^2*Gk3^2*Gk4^2);
Phasead = ((s+30))/((s+400));

%#################################################################
%Compensation links for the 23'rd to the 31'st actuator
%Family 5
%#################################################################

K=5e5; %Static gain
s=tf('s'); %Specifies the transfer function H(s) = s
```

```
%Compensation links
Phasead = ((s+6))/((s+200));

sys = K*Phasead*Gsys; %The compensated system

%The controller
[numreg23to31,denreg23to31] = tfdata(K*Phasead,'v');

%#################################################################
%Compensation links for the 32'nd actuator - Family 6
%#################################################################

K=6.2; %Static gain
w1=7; %Locations for the inverted Notch filters
w2=15;
w3=50;
w4=150;
z=0.25; %Damping for the inverted Notch filters
s=tf('s'); %Specifies the transfer function H(s) = s

%Transfer functions for the inverted Notch filters
Gk1 = K*(s+w1)^2/((s)^2+2*z*w1*s+w1^2);
Gk2 = K*(s+w2)^2/((s)^2+2*z*w2*s+w2^2);
Gk3 = K*(s+w3)^2/((s)^2+2*z*w3*s+w3^2);
Gk4 = K*(s+w4)^2/((s)^2+2*z*w4*s+w4^2);

%Compensation links
Bandpas=(Gk1^2*Gk2^1*Gk3^1*Gk4^1);
Phasead = ((s+6))/((s+800));
Phasedec=(s+4)^2/((s+0.01)^2);

sys = K*Bandpas*Phasead*Phasedec*Gsys; %The compensated system

%The controller
[numreg32,denreg32] = tfdata(K*Bandpas*Phasead*Phasedec,'v');
```

A.5 Create a movie of the mirror

```
%#################################################################
%Creates a motion picture of the deformations clarifying the
%dynamics of the full mirror
%Authors: Fredrik Bjöörn & Olof Garpinger
%#################################################################
load M2-modal_a_modes
%Load deformations and time scale from mirror simulations
load Output

%The big model does not use nodes 1 to 6
x = a_modes(7:end,2); %x-coordinates
y = a_modes(7:end,3); %y-coordinates
clear a_modes %Memory allocation

%The first row in y16643 is the time vector
dz = y16643(2:3163,1:length(y16643(1,:))); %Only deformations
tri = delaunay(x,y); %Delaunay triangulation

%Making a full screen figure that presents the movie
bdwidth=5;
set(0,'Units','pixels')
pos=[bdwidth, 650, 1024, 650];
figure('Position', pos)

%Uppdates the figure with new deformations for every time
%sample
for i = 1:length(y16643(1,:))
  %Triangular surface plot, no edge lines
  trisurf(tri,x,y,dz(:,i),'EdgeColor','none')
    shading interp
    axis([-2.5 2.5 -2.5 2.5 -12e-5 4e-5])
    xlabel(['time : ' num2str(y16643(1,i)) 's'])
    view(0,30)
    pause(0.05) %Uppdate the figure every 0.05 s
end
```

A.6 Initial file to test full mirror step responses

```
%#################################################################
%This script initializes the matrices used in the control of
%the full mirror model
%Authors: Fredrik Bjöörn & Olof Garpinger
%#################################################################
clear
%Load the different controllers used on the full mirror
load ControllerV6 numreg denreg
load Controller32FredrikV6 numreg32 denreg32
%Load a matrix containing the force distributions, different
%force vector depending on where on the mirror the local
%model is placed
load ForcevectorV6 force

s=tf('s');
%Controller used for local control of sections
Gk=tf(numreg,denreg);
%Controller for local control of smaller sections
Gk31=20*tf(numreg32,denreg32);
%Controller used for SISO control of the edge
Gk32=6*tf(numreg32,denreg32);


Gr=Gk;
%Retrieving controller state space matrices
Regsys=ss(Gr);
Ar=Regsys.a;
Br=Regsys.b;
Cr=Regsys.c;
Dr=Regsys.d;

ArR=length(Ar); %Order of the section controller

%The same controller is used for the third ring from the edge
%as for the rings located from here to the center
GrW2Rings=Gk;
%Retrieving controller state space matrices
RegsysW2Rings=ss(GrW2Rings);
ArW2Rings=RegsysW2Rings.a;
```

```
BrW2Rings=RegsysW2Rings.b;
CrW2Rings=RegsysW2Rings.c;
DrW2Rings=RegsysW2Rings.d;

ArW2RingsR=length(ArW2Rings); %Order of the section controller

%Controller used for local control of smaller sections
Gr31=Gk31;
%Retrieving controller state space matrices
Regsys31=ss(Gr31);
Ar31=Regsys31.a;
Br31=Regsys31.b;
Cr31=Regsys31.c;
Dr31=Regsys31.d;

Ar31R=length(Ar31); %Order of the smaller section controller

Gr32=Gk32;
%Retrieving A, B, C and D matrices for the SISO controller
Regsys32=ss(Gr32);
Ar32=Regsys32.a;
Br32=Regsys32.b;
Cr32=Regsys32.c;
Dr32=Regsys32.d;

Ar32R=length(Ar32); %Order of the SISO controller

%-------------------------------------------------------------
%Build matrices so that the controllers can
%control the full mirror
%-------------------------------------------------------------
Aregtemp = sparse(2592*ArR,2592*ArR);
Bregtemp = sparse(2592*ArR,2592);
Cregtemp = sparse(2592*19,2592*ArR);
Dregtemp = sparse(2592*19,2592);
%6 more in each ring

%Put the local model section controller matrices in the
%"diagonal" of new controller matrices
l = 1; %Force distibution counter
j = 1; %Matrix counter
```

```
k = 1; %force vector counter
n = 43;
m = 24;

for i = 1:2592 % for all actuators controlled by large sections

    %Choose the correct k-value for the force matrix
    %For all actuators placed between the center and the third
    %ring to the edge
    if i < 43 | i > 2418

    elseif n == i %To get the right force vector

        k = k+1; %Force vector counter
        n = i+m+6;
        m = m+6;

    end

    Aregtemp(j:j+length(Ar)-1,j:j+length(Ar)-1) = Ar;
    Bregtemp(j:j+length(Ar)-1,i) = Br;
    Cregtemp(l:l+19-1,j:j+length(Ar)-1) = forcemat(:,k)*Cr;
    Dregtemp(l:l+19-1,i) = forcemat(:,k)*Dr;
    j = j + length(Ar);
    l = l + 19;

    if i == 42
        k = 0;
    end

end

l = 1;
j = 1; %Matrix counter

AregW2Rings = sparse(ArW2RingsR*180,ArW2RingsR*180);
BregW2Rings = sparse(ArW2RingsR*180,180);
CregW2Rings = sparse(180*19,ArW2RingsR*180);
DregW2Rings = sparse(180*19,180);

for i = 1:180 % for all actuators in the third ring
```

```
    AregW2Rings(j:j+length(ArW2Rings)-1,j:j+length(ArW2Rings)-1) = ArW2Rings;
    BregW2Rings(j:j+length(ArW2Rings)-1,i) = BrW2Rings;
    CregW2Rings(l:l+19-1,j:j+length(ArW2Rings)-1) = forcemat(:,24)*CrW2Rings;
    DregW2Rings(l:l+19-1,i) = forcemat(:,24)*DrW2Rings;
    j = j + length(ArW2Rings);
    l = l + 19;

end

j = 1; %Matrix counter

Areg31 = sparse(Ar31R*186,Ar31R*186);
Breg31 = sparse(Ar31R*186,186);
Creg31 = sparse(186,Ar31R*186);
Dreg32 = sparse(186,186);

for i = 1:186 % for all actuators in the second ring from the edge

    Areg31(j:j+length(Ar31)-1,j:j+length(Ar31)-1) = Ar31;
    Breg31(j:j+length(Ar31)-1,i) = Br31;
    Creg31(i,j:j+length(Ar31)-1) = Cr31;
    Dreg31(i,i) = Dr31;
    j = j + length(Ar31);

end

j = 1; %Matrix counter

Areg32 = sparse(Ar32R*192,Ar32R*192);
Breg32 = sparse(Ar32R*192,192);
Creg32 = sparse(192,Ar32R*192);
Dreg32 = sparse(192,192);

for i = 1:192 % for all actuators positioned at the edge

    Areg32(j:j+length(Ar32)-1,j:j+length(Ar32)-1) = Ar32;
    Breg32(j:j+length(Ar32)-1,i) = Br32;
    Creg32(i,j:j+length(Ar32)-1) = Cr32;
    Dreg32(i,i) = Dr32;
    j = j + length(Ar32);
```

```
end

%Matrices are temporary saved for memory allocation
save RegmatricesW2MRingsV6 Aregtemp Bregtemp Cregtemp Dregtemp...
 AregW2Rings BregW2Rings CregW2Rings DregW2Rings Areg31 Breg31...
  Creg31 Dreg31 Areg32 Breg32 Creg32 Dreg32

save dimensionsV6 ArR ArW2RingsR Ar31R Ar32R

clear
load RegmatricesW2MRingsV6
load dimensionsV6

%-------------------------------------------------------------
%New matrices that will contain all control matrices
%-------------------------------------------------------------
Areg=sparse(2592*ArR+ArW2RingsR*180+Ar31R*186+Ar32R*192,...
 2592*ArR+ArW2RingsR*180+Ar31R*186+Ar32R*192);
Breg=sparse(2592*ArR+ArW2RingsR*180+Ar31R*186+Ar32R*192,...
 2592+180+186+192);
Creg=sparse(2592*19+180*19+186+192,...
 2592*ArR+ArW2RingsR*180+Ar31R*186+Ar32R*192);
Dreg=sparse(2592*19+180*19+186+192,...
 2592+180+186+192);

Areg=[Aregtemp zeros(2592*ArR,...
 ArW2RingsR*180+Ar31R*186+Ar32R*192);...
 zeros(ArW2RingsR*180,2592*ArR) AregW2Rings ...
 zeros(ArW2RingsR*180,Ar31R*186+Ar32R*192);...
 zeros(Ar31R*186,2592*ArR+ArW2RingsR*180)...
 Areg31 zeros(Ar31R*186,Ar32R*192);...
 zeros(Ar32R*192,2592*ArR+ArW2RingsR*180+Ar31R*186) Areg32];

Breg=[Bregtemp zeros(2592*ArR,180+186+192);...
 zeros(ArW2RingsR*180,2592) BregW2Rings...
 zeros(ArW2RingsR*180,186+192);...
 zeros(Ar31R*186,2592+180) Breg31 zeros(Ar31R*186,192);...
 zeros(Ar32R*192,2592+180+186) Breg32];

Creg=[Cregtemp zeros(2592*19,...
```

```
 ArW2RingsR*180+Ar31R*186+Ar32R*192);...
 zeros(180*19,2592*ArR) CregW2Rings...
 zeros(180*19,Ar31R*186+Ar32R*192);...
 zeros(186,2592*ArR+ArW2RingsR*180)...
 Creg31 zeros(186,Ar32R*192);...
 zeros(192,2592*ArR+ArW2RingsR*180+Ar31R*186) Creg32];

Dreg=[Dregtemp zeros(2592*19,180+186+192);...
 zeros(180*19,2592) DregW2Rings zeros(180*19,186+192);...
 zeros(186,2592+180) Dreg31 zeros(186,192);...
 zeros(192,2592+180+186) Dreg32];

save RegmatricesRings3To30And32V6 Areg Breg Creg Dreg

clear %Memory allocation
load RegmatricesRings3To30And32V6 Areg Breg Creg Dreg

%Feed the right deformations back
I=sparse([zeros(2772,12) eye(2772) zeros(2772,192+186);...
 zeros(186,12+2772) eye(186) zeros(186,192);...
 zeros(192,12+2772+186) eye(192)]);

I = sparse([I zeros(3150,3162)]);
R=zeros(3162-12,1);
%Step response reference
nbntemp=getNeighbourRings(16643)-18;
R(nbntemp(1))=0.6;
R(nbntemp(2:7))=0.5;
R(nbntemp(8:19))=0.25;

%Distributing the forces to right actuators
load PmatrixOlofV6
P = [P [zeros(3168-192-186,186);...
 eye(186);zeros(192,186)] [zeros(3168-192,192);eye(192)]];
P = P(7:3168,:);

%Feedback of velocities
load LmatrixV6
Lmat = Lmat(7:3168)';
I2 = sparse([zeros(3162) eye(3162)]);
Lmat = diag(full(Lmat*I2));
```

```
Lmat=Lmat(end/2+1:end,:)./2;

pack %Memory allocation
load TorbenBigModelV6 %The full mirror model

%Get velocities as outputs from the mirror model
Cm2 = sparse([Cm(:,1:3354) zeros(3162,3354);...
 zeros(3162,3354) Cm(:,1:3354)]);
clear Cm
```

A.7 Place forces on the deformable mirror

```
%#################################################################
%Makes sure the forces are distributed to the right actuators
%Authors: Fredrik Björn & Olof Garpinger
%#################################################################
%Load the neigbour rings for the activated actuators
load nbnRingsMatrixW2Rings2 nbnMatrix1 nbnMatrix2
nbnMatrix2=[nbnMatrix2(:,1) nbnMatrix2(:,3) nbnMatrix2(:,2)...
 nbnMatrix2(:,7) nbnMatrix2(:,6) nbnMatrix2(:,5) nbnMatrix2(:,4)];

load M2-modal_a_modes
a_modes=a_modes(:,1);

%Force distribution to nineteen actuators
for i=1:18
    temp(i,1:19)=getNeighbourRings(a_modes(i+18))';
end

j = 1; %Row counter in nbnMatrix
l = 1; %Column counter in nbnMatrix
P1 = sparse(3168,52668); %Create sparse matrix
nbnMatrix1=[temp;nbnMatrix1];

for i=1:52668

    %In Column nbr i put 1 in the row corresponding
    %to the current actuator
    P1(nbnMatrix1(j,l),i)=1;

    if l == 19 %Change row in nbnMatrix
        l = 1;
        j = j+1;

    else %Change Column in nbnMatrix
        l = l+1;
    end

end

j = 1; %Row counter in nbnMatrix
```

```
l = 1; %Column counter in nbnMatrix
P2 = sparse(3168,1302); %Create sparse matrix

for i=1:1302

  %In Column nbr i put 1 in the row corresponding
  %to the current actuator
    P2(nbnMatrix2(j,l),i)=1;

    if l == 7 %Change row in nbnMatrix
        l = 1;
        j = j+1;

    else %Change Column in nbnMatrix
        l = l+1;
    end

end

P=sparse(3168,52668+1302);
P=[P1 P2];
save PmatrixV6 P -v6
```